

Article

Novel Advanced Artificial Neural Network-Based Online Stator and Rotor Resistance Estimator for Vector-Controlled Speed Sensorless Induction Motor Drives

Ajithanjaya Kumar Mijar Kanakabettu ^{1,2,*} , Rajkiran Ballal Irvathoor ³, Sanath Saralaya ¹, Sathyendra Bhat Jodumutt ⁴  and Athokpam Bikramjit Singh ⁵

¹ Department of Electrical and Electronics Engineering, St. Joseph Engineering College, Mangalore 575028, India; sanaths@sjec.ac.in

² Department of Electrical and Electronics, Nitte Meenakshi Institute of Technology, Bengaluru 560064, India

³ Department of Electrical and Electronics Engineering, Channabasaveshwara Institute of Technology, Tumkur 572216, India; rajakiranballali@cittumkur.org

⁴ Department of Computer Applications, St. Joseph Engineering College, Mangalore 575028, India; sathyendrab@sjec.ac.in

⁵ Department of Computer Science and Engineering, Yenepoya Institute of Technology, Mangalore 574225, India; bikramjits@yit.edu.in

* Correspondence: ajithk@sjec.ac.in; Tel.: +91-9945251967

Abstract: This paper presents a new approach for the online estimation of stator and rotor resistance of induction motors for speed sensorless vector-controlled drives, using feed-forward artificial neural networks with advanced adaptive learning rates. For the rotor resistance estimation, a neural network model based on rotor speed and stator currents is developed. The rotor flux linkages acquired from the voltage model are compared with the neural network model. The feed-forward neural network employs an adaptive learning rate as the function of the obtained error during training for quick convergence with minimal estimation error. A two-layered neural network model based on the stator voltage and current equations is developed for the stator resistance estimation. The d-q axes stator currents obtained from the developed model are compared with the acquired d-q axes stator currents. For the fast convergence with minimal estimation error, an adaptive learning rate as the function of error is adopted during training. Furthermore, the neural network estimates the induction motor's speed. The simulation and experimental results justify that the developed algorithms track variation in the resistances quickly and precisely along with the speed as compared with the conventional constant learning rate algorithm, leading to reliable operation of the drive.

Keywords: artificial neural network; speed sensorless vector-controlled drives; adaptive learning rate; stator resistance; rotor resistance



Citation: Kanakabettu, A.K.M.; Irvathoor, R.B.; Saralaya, S.; Jodumutt, S.B.; Singh, A.B. Novel Advanced Artificial Neural Network-Based Online Stator and Rotor Resistance Estimator for Vector-Controlled Speed Sensorless Induction Motor Drives. *Energies* **2024**, *17*, 2150. <https://doi.org/10.3390/en17092150>

Academic Editor: Marcin Kaminski

Received: 24 February 2024

Revised: 23 April 2024

Accepted: 26 April 2024

Published: 30 April 2024



Copyright: © 2024 by the authors. Licensee MDPI, Basel, Switzerland. This article is an open access article distributed under the terms and conditions of the Creative Commons Attribution (CC BY) license (<https://creativecommons.org/licenses/by/4.0/>).

1. Introduction

Induction motors are extensively used motors in industrial environments due to their enormous advantages over similar categories of motors. Due to the vast advantages of excellent performance, rigorousness, and minimal maintenance, induction motors are the best alternative for DC motors. The speedy development in semiconductor and control technologies resulted in replacing DC motors with induction motors for similar applications in most industries. With the advancement in power electronics, the majority of speed control-related issues have been resolved. Nearly half of the energy generated in the world is consumed by electrical drives. Improvement in the energy efficiency of the drive systems is of great concern, where a minute improvement in energy efficiency reduces power loss and fuel burn [1]. Inverter-fed induction motors are extensively used for speed control where the stability of the drive is of more significant concern and is to be addressed together with the solutions to reduce energy consumption [2–5].

The scalar and vector control strategies are generally employed for the speed control of Induction Motor Drives (IMD); even though they are easy to implement, scalar-controlled drives suffer from inherent coupling effects and sluggish response, and are extremely prone to system instability. Despite the involvement of a complex control strategy, vector control or field orientation control has a wide range of advantages; a few are better dynamic response, higher efficiency over a wide range of speed, exploiting full torque capability at low speeds, and decoupled control of flux and torque [6]. With regard to field orientation control, accurate estimation of machine parameters is essential to achieving an excellent dynamic response as the slip relation is essential for the implementation of an indirect field-oriented scheme, which is a feed-forward technique, parameter sensitive especially to rotor resistance. The determination of rotor speed depends on the rotor flux estimation. The influence of rotor resistance on the estimation of rotor flux, which is the essential control parameter, is extremely significant [7]. For the speed estimation employing an induction motor model, accurate estimation of the motor parameters is essential. To achieve minimal speed estimation error and to eliminate the unstable operation of the drive, online stator resistance estimation is needed. With the rotor heating, rotor resistance can rise to 100%. It is highly undesirable to obtain rotor resistance value with the temperature sensor or thermal model [8].

Several rotor and stator resistance estimation algorithms are available in the literature. The most popular approaches are based on Extended Kalman Filters (EKFs) [9–13], the Model Reference Adaptive System (MRAS) [14–16], Sliding Mode Control [17–19], Luenberger Observer [20–22], and artificial intelligence-based techniques such as artificial neural networks [23,24] fuzzy—neural networks, etc. [25,26]. In recent days, several modifications have been proposed to the traditional methods with different combinations as available in the recent literature. The MRAS approach for the estimation of machine parameters is popular as the other traditional approaches are computationally intensive, with noise influence and complexity in practical realization.

Several MRAS-based techniques are available for the control of sensorless vector-controlled IMD, which are primarily based on the error minimization of the signals as Rotor flux error-based MRAS [27,28], Back-EMF error-based MRAS [29,30], Reactive power error-based MRAS [31–33], Stator current error-based MRAS [34,35], X-MRAS [36,37], and High-Frequency Injection Method (HFIM) based MRAS [38–40]. The conventional MRAS approach uses an integral or proportional-integral controller. Since the modern high-speed DSPs have made the implementation of computationally intensive tools such as Artificial Neural Network (ANN), fuzzy logic, etc. simple, modern advanced MRAS techniques incorporate ANN and fuzzy logic. The literature is available on the review of the performance of various MRAS-based techniques [41,42].

As ANNs are capable of approximating nonlinear functions with a great degree of accuracy, their application for identifying and controlling nonlinear dynamic systems is increased. The replacement of the adaptive model of conventional RF-MARS by neural networks in speed estimation of IMD reduces the computational efforts and is also immune to the effect of stator and rotor resistance variation on the system. A great improvement in the performance of the speed estimator is achieved, particularly at low speeds, both with open-loop and closed-loop conditions [43,44]. The online rotor and stator resistance estimation approaches are proposed, where a fixed learning rate is adopted during the estimation approach [45,46]. The selection of an inappropriate learning rate leads to output errors with slow convergence of the error during network training.

The online artificial neural network-based MRAS-based stator and rotor resistance estimator employing varying learning rates throughout the training as a function of obtained error during training is proposed. The adjustable learning rate based on the error function reduces the estimation time and improves the induction motor drive's control quality. Both the stator and rotor resistance estimators, shown in Figure 1, make use of two state estimate variable models: one delivers the induction motor's real output states, while the subsequent one provides corresponding neural network model states. The error

obtained between the output states of the two models is back propagated by adjusting the weights of the neural network model until the error between the output states of the two models reaches the acceptable minimum value. The weights obtained at the end of the training are used to estimate the resistance values. The standard two-layer feed-forward neural network model and two-layer recurrent feed-forward neural network model are employed for the rotor and stator resistance estimations, respectively. The effectiveness of the developed rotor and stator estimators for the online estimation is justified by the simulation studies performed on the stator reference frame model of an induction motor using MATLAB-SIMULINK and presented. The motor parameters of a 3.7 kW induction motor are determined by performing the no-load and blocked rotor tests and developing the equivalent circuit. The performance of the developed algorithms for the online estimation of stator and rotor resistances, along with speed estimation, are tested experimentally on a 3.7 kW squirrel cage induction motor drive operated with rotor flux orientation controller. The experimental results demonstrate the capability of the proposed algorithm to estimate resistances along with speed precisely.

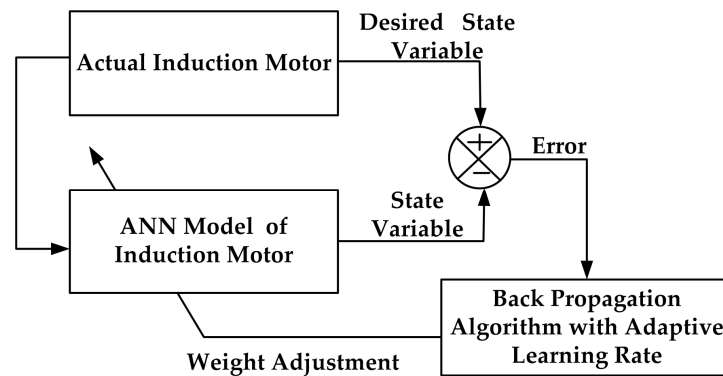


Figure 1. An ANN-based Model Reference Adaptive System for identifying parameters [7].

2. Artificial Neural Network-Based Rotor Resistance Estimator

The ANN-based MRAS structure for the rotor resistance estimation is presented in Figure 2.

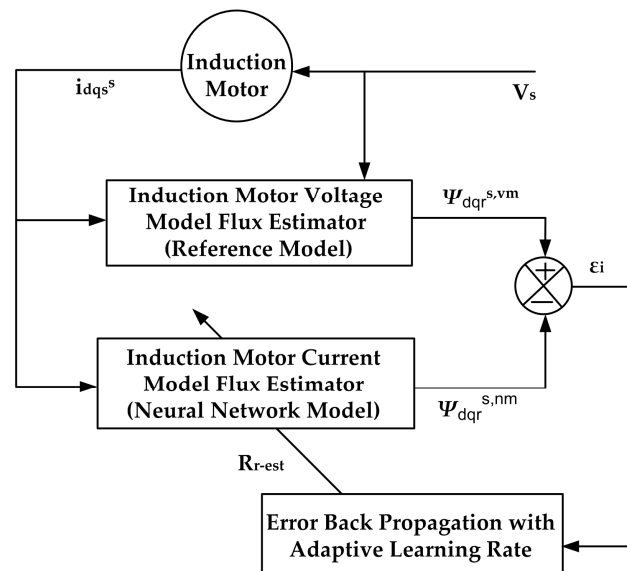


Figure 2. ANN-based MRAS structure for rotor resistance estimation [7].

The rotor flux vectors are estimated by two separate observers depicted as the voltage model and current model of the induction motor. The d - and q -axes rotor flux equations are

derived by assessing the stator side of the equivalent circuit developed from the stationary reference frame model as in Equation (1), referred to as the voltage model equation [47,48].

$$\begin{bmatrix} \frac{d\psi_{dr}^s}{dt} \\ \frac{d\psi_{qr}^s}{dx} \end{bmatrix} = \frac{L_r}{L_m} \left\{ \begin{bmatrix} v_{ds}^s \\ v_{qs}^s \end{bmatrix} - R_s \begin{bmatrix} i_{ds}^s \\ i_{qs}^s \end{bmatrix} - \sigma L_s \begin{bmatrix} \frac{d}{dt} i_{ds}^s \\ \frac{d}{dt} i_{qs}^s \end{bmatrix} \right\} \tag{1}$$

where $\sigma = 1 - \frac{L_m^2}{L_s L_r}$ is the leakage factor of the machine.

By assessing the rotor side of the equivalent circuit, the d - q axes rotor flux equations, also known as current or neural network model equation, is obtained, represented in Equation (2).

$$\frac{d}{dt} \overrightarrow{\psi_r^{s,im}} = \left[-\frac{1}{T_r} I + \omega_r J \right] \overrightarrow{\psi_r^{s,im}} + \frac{L_m}{T_r} \overrightarrow{i_{dq}^s} \tag{2}$$

where $T_r = \frac{L_r}{R_r}$ is the rotor time constant,

$$I = \begin{bmatrix} 1 & 0 \\ 0 & 1 \end{bmatrix}; J = \begin{bmatrix} 0 & -1 \\ 1 & 0 \end{bmatrix}; \overrightarrow{i_{dq}^s} = \begin{bmatrix} i_{ds}^s \\ i_{qs}^s \end{bmatrix}; \overrightarrow{\psi_r^{s,im}} = \begin{bmatrix} \psi_{dr}^{s,im} \\ \psi_{qr}^{s,im} \end{bmatrix}; \overrightarrow{\psi_r^{s,vm}} = \begin{bmatrix} \psi_{dr}^{s,vm} \\ \psi_{qr}^{s,vm} \end{bmatrix}$$

The sample data model of Equation (2) is represented by Equation (3) as

$$\overrightarrow{\psi_r^{s,vm}}(k) = (W_1 I + W_2 J) \overrightarrow{\psi_r^{s,vm}}(k-1) + W_3 \overrightarrow{i_{dq}^s} \tag{3}$$

where $W_1 = 1 - \frac{T_s}{T_r}$; $W_2 = \omega_r T_s$ and $W_3 = \frac{L_m}{T_r} T_s$.

T_s is sampling time.

Equation (3) can be represented as

$$\overrightarrow{\psi_r^{s,vm}} = W_1 X_1 + W_2 X_2 + W_3 X_3 \tag{4}$$

where $X_1 = \begin{bmatrix} \psi_{dr}^{s,vm}(k-1) \\ \psi_{qr}^{s,vm}(k-1) \end{bmatrix}$; $X_2 = \begin{bmatrix} -\psi_{qr}^{s,vm}(k-1) \\ \psi_{dr}^{s,vm}(k-1) \end{bmatrix}$; $X_3 = \begin{bmatrix} i_{ds}^s(k-1) \\ i_{qs}^s(k-1) \end{bmatrix}$.

Based on Equation (4), a two-layer neural network is developed, presented in Figure 3. X_1 , X_2 , and X_3 represent the inputs to the network, and W_1 , W_2 , and W_3 represent the network weights. Since W_2 is independent of the rotor resistance term, during the training of the network, weights W_1 and W_3 are required to be updated.

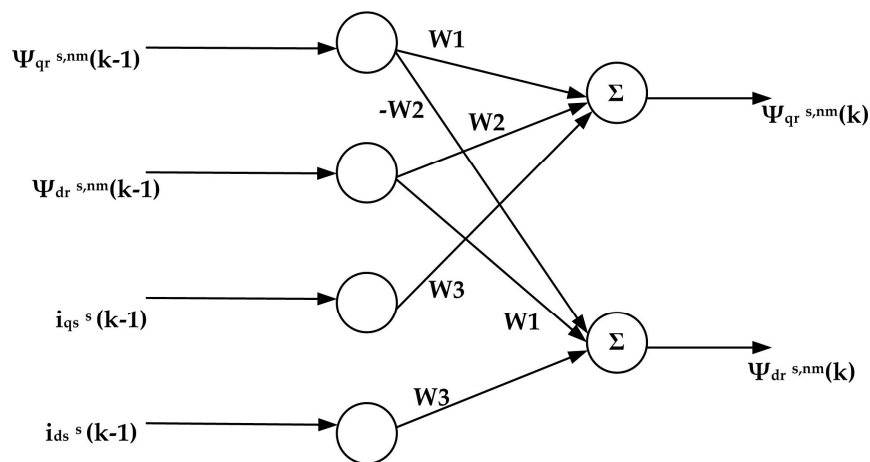


Figure 3. Implementation of the current model for rotor flux by two-layered neural network [8].

The square function of the rotor flux error between the reference model and the neural network model is

$$E_r = \frac{1}{2} \epsilon_r^2(k) = \frac{1}{2} \left\{ \overrightarrow{\psi_r^{s,vm}} - \overrightarrow{\psi_r^{s,nm}} \right\}^2 \quad (5)$$

During training, weights W_1 and W_3 are updated to obtain the minimum square function as

$$W_1(k) = W_1(k-1) + \eta_1 \Delta W_1(k) \quad (6)$$

$$W_3(k) = W_3(k-1) + \eta_3 \Delta W_3(k) \quad (7)$$

Using the generalized delta rule, the weight adjustment factors $\Delta W_1(k)$ and $\Delta W_3(k)$ are evaluated as

$$\Delta W_1(k) = -\frac{\partial E_r}{\partial W_1} = \left[\overrightarrow{\psi_r^{s,vm}}(k) - \overrightarrow{\psi_r^{s,nm}}(k) \right]^T \overrightarrow{\psi_r^{s,nm}}(k-1) \quad (8)$$

$$\Delta W_3(k) = -\frac{\partial E_r}{\partial W_3} = \left[\overrightarrow{\psi_r^{s,vm}}(k) - \overrightarrow{\psi_r^{s,nm}}(k) \right]^T \overrightarrow{i_{dq}^s}(k-1) \quad (9)$$

With experience gained from the repeated training of the network, learning rates η_1 and η_2 are selected to obtain a minimum error.

The adaptive learning rate algorithm is developed, where the adaptive learning rate substitutes the constant learning rate throughout the training, for quick convergence and reduced estimate error. During each training iteration, weights are updated based on the modified learning rate to reduce the error E_r . The learning rate is updated during training determined by the product of weight adjustment factors at k and $(k-1)$ iteration given by $\varphi_i(k) = \Delta W_i(k) \times \Delta W_i(k-1)$.

By using the bipolar sigmoid function as given in Equation (10), the learning rate for the k th iteration during learning is computed.

$$f(\varphi_i(k)) = \alpha_i \frac{1 - e^{-s \cdot \varphi_i(k)}}{1 + e^{-s \cdot \varphi_i(k)}} \quad (10)$$

where s is the steepness parameter, which may vary between -1 and $+1$; α_i is the positive constant.

Considering the learning rate of $(k-1)$ iteration, the updated learning rate for the k th iteration is obtained from

$$\eta_i(k) = \eta_i(k-1) * [1 + f(\varphi_i(k))] \quad (11)$$

With the updated learning rate as obtained from Equation (11), the weights W_1 and W_3 updated are as per Equations (6) and (7).

At the end of the training, rotor resistance R_{r-est} is estimated by considering either W_1 or W_3 as per Equations (12) or (13) as

$$R_{r-est} = \frac{L_r W_3}{L_m T_s} \quad (12)$$

$$R_{r-est} = \frac{L_r (1 - W_1)}{T_s} \quad (13)$$

The d and q axes rotor fluxes estimated from the voltage model depend on the stator resistance R_s as given in Equation (1). To minimize the error in rotor resistance estimation, an online stator resistance estimator is developed and is presented in Section 3.

3. Artificial Neural Network-Based Stator Resistance Estimator

The equations corresponding to voltage and current models used in rotor resistance estimation [7], represented as Equations (1) and (2), are used to obtain the d and q axes currents of the induction motor as

$$\frac{d}{dt} i_{ds}^s = \frac{L_m}{\sigma L_s L_r T_r} \psi_{dr}^s + \frac{L_m}{\sigma L_s L_r} \omega_r \psi_{qr}^s - \frac{L_m^2}{\sigma L_s L_r T_r} i_{ds}^s + \frac{1}{\sigma L_s} v_{ds}^s - \frac{1}{\sigma L_s} R_s i_{ds}^s \quad (14)$$

$$\frac{d}{dt} i_{qs}^s = \frac{L_m}{\sigma L_s L_r T_r} \psi_{qr}^s - \frac{L_m}{\sigma L_s L_r} \omega_r \psi_{dr}^s - \frac{L_m^2}{\sigma L_s L_r T_r} i_{qs}^s + \frac{1}{\sigma L_s} v_{qs}^s - \frac{1}{\sigma L_s} R_s i_{qs}^s \quad (15)$$

Equations (14) and (15) are expressed in discrete form as

$$i_{ds}^{s*}(k) = W_4 i_{ds}^s(k-1) + W_5 \psi_{dr}^s(k-1) + W_6 \psi_{qr}^s(k-1) + W_7 v_{ds}^s(k-1) \quad (16)$$

$$i_{qs}^{s*}(k) = W_4 i_{qs}^s(k-1) + W_5 \psi_{qr}^s(k-1) - W_6 \psi_{dr}^s(k-1) + W_7 v_{qs}^s(k-1) \quad (17)$$

where $W_4 = \left[1 - \left(\frac{T_s}{\sigma L_s} \right) R_s - \left(\frac{L_m^2}{L_r T_r} \right) \left(\frac{T_s}{\sigma L_s} \right) \right]$; $W_5 = \left(\frac{L_m}{L_r T_r} \right) \left(\frac{T_s}{\sigma L_s} \right)$; $W_6 = \left(\frac{L_m}{L_r} \right) \left(\frac{T_s}{\sigma L_s} \right) \omega_r$; $W_7 = \frac{T_s}{\sigma L_s}$.

A two-layer recurrent neural network, as shown in Figure 4, is developed from Equations (16) and (17) for the stator current estimation. The * indicates the estimated values in neural network model.

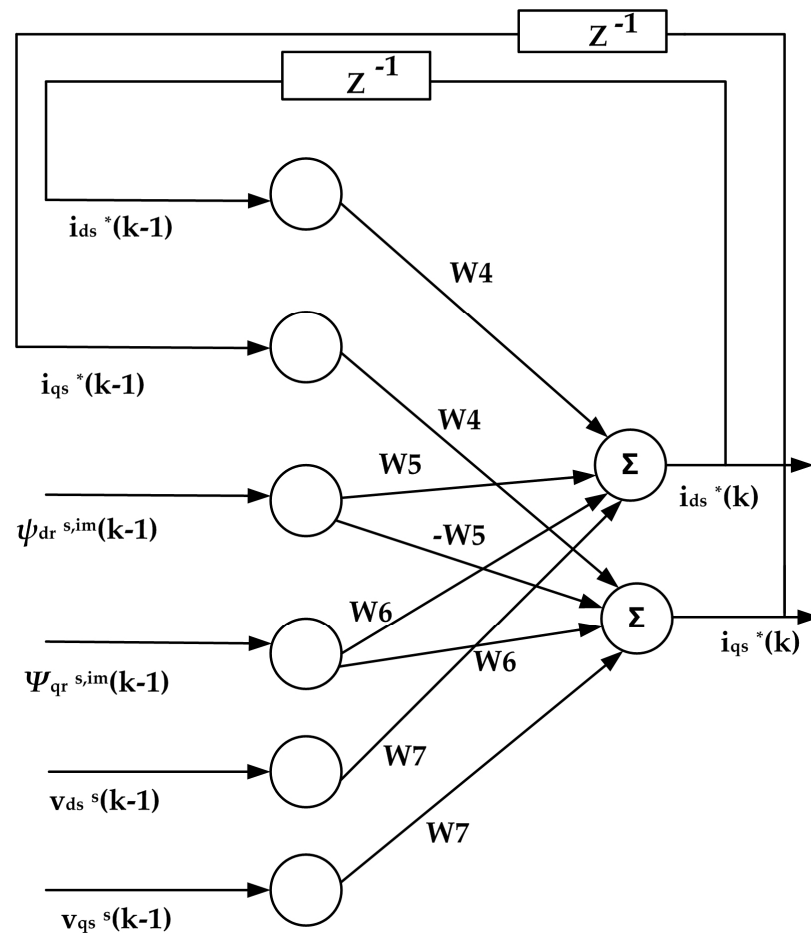


Figure 4. Two-layered Recurrent Neural Network Model for d and q axes stator current estimation [48].

The weights W_5 , W_6 , and W_7 are obtained from machine parameters, sampling interval T_s , and rotor speed ω_r . During the network training, only W_4 is adjusted, as other weights

are independent of stator resistance. The standard back-propagation algorithm is adopted for the training of the neural network.

The square function of the stator current error between the reference model and the neural network model is

$$E_s = \frac{1}{2} \vec{\epsilon}_s^2(k) = \frac{1}{2} \{i_s(k) - i_s^*(k)\}^2 \tag{18}$$

To obtain the minimal error square function E_s , Weight W_4 is updated during training as

$$W_4(k) = W_4(k - 1) + \eta_4 \Delta W_4(k) \tag{19}$$

Based on the repeated training performed on the network, with trial and error, the initial learning rate η_4 is selected. The weight adjustment factor $\Delta W_4(k)$ is obtained as

$$\Delta W_4(k) = -\frac{\partial E_s}{\partial W_4} = \left[\vec{i}_s(k) - \vec{i}_s^*(k) \right]^T * \vec{i}_s^*(k-1) \tag{20}$$

The constant learning rate is replaced by an adaptive learning rate based on the bipolar sigmoid function. The learning rate is updated during the training as

$$\eta_4(k) = \eta_4(k - 1) * [1 + f(\varphi_i(k))] \tag{21}$$

where $\varphi_i(k) = \Delta W_4(k) \times \Delta W_4(k - 1)$.

The function $f(\varphi_i(k))$ is determined by adopting the activation function as explained for the rotor resistance estimation in Section 2.

Considering the adjustment weight W_4 obtained at the end of the training, the stator resistance is estimated as

$$R_{s-est} = \left\{ 1 - W_4 - \frac{T_s}{\sigma L_s} \frac{L_m^2 R_r}{L_r^2} \right\} \frac{\sigma L_s}{T_s} \tag{22}$$

The stator resistance is thus estimated by the ANN-based MRAS estimator, as shown in Figure 5.

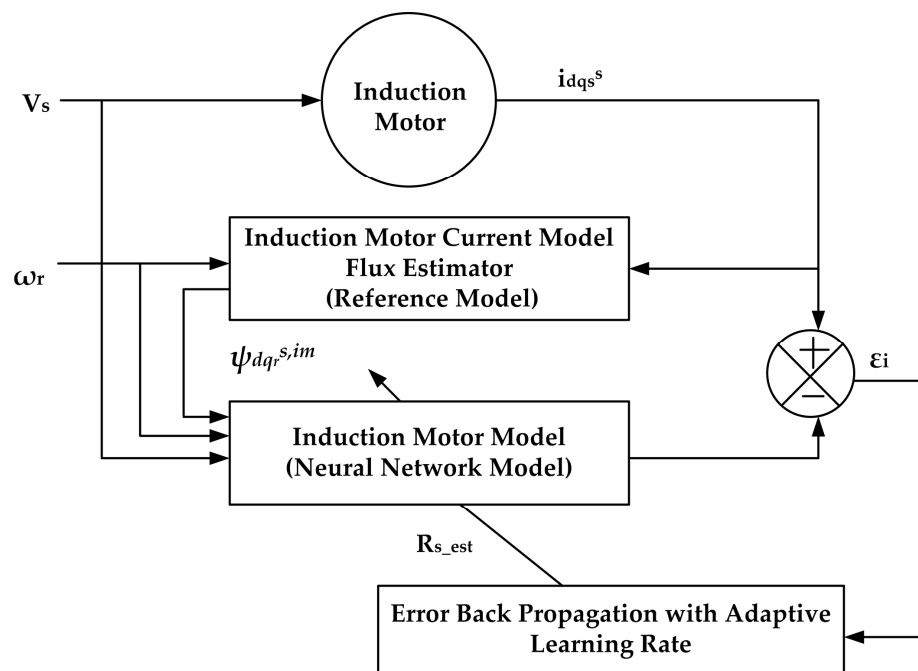


Figure 5. ANN-based MRAS structure for stator resistance estimation [48].

The speed of the sensorless drive is estimated as shown in [8] given below as

$$\omega_{r-est} = \omega_{r-est}(k-1) + \frac{\eta_{sp}}{T_s} \left\{ \begin{array}{l} \left[\psi_{qr}^{s,vm}(k) - \psi_{qr}^{s,im}(k) \right] \psi_{dr}^{s,im}(k-1) \\ - \left[\psi_{dr}^{s,vm}(k) - \psi_{dr}^{s,im}(k) \right] \psi_{qr}^{s,im}(k-1) \end{array} \right\} \quad (23)$$

where η_{sp} is the learning rate for rotor speed estimation, and T_s is the sampling time.

4. Results and Discussion

The machine parameters of the induction motor with 3.7 kW are determined in the laboratory by performing the no-load and blocked rotor tests. With the obtained parameters, the performance of the proposed algorithm for online stator and rotor resistance is evaluated by the simulation and with the hardware setup, as presented in the following sections, followed by a discussion of the results.

4.1. Tests for Identification of Machine Parameters

The resistance of stator windings is evaluated by the volt-amp test. The no-load, locked rotor tests are performed to determine equivalent circuit parameters. The experiments are performed using the machine specified by the nameplate information provided in Table 1. Figure 6 illustrates the experimental setup employed in the laboratory for the determination of machine characteristics.

Table 1. Induction motor information.

Power (HP)	3.7 kW
Current (Amps)	7.5
Terminal voltage (Volts)	415
Frequency (Hz)	50
Poles	4
No-load speed (RPM)	1498
Stator connection	Delta

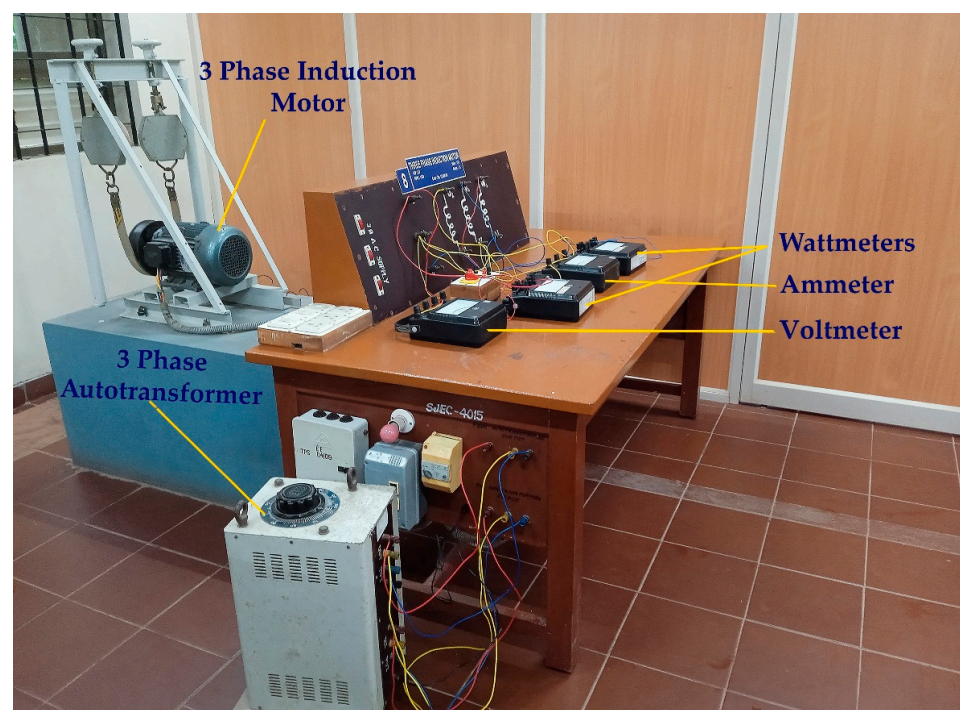


Figure 6. Experimental setup for locked rotor and no-load test.

4.1.1. Stator Winding Resistance Estimation

The low voltage DC is applied to one of the phase windings of three-phase winding, as shown in Figure 7. Calculating DC resistance requires taking the data from both an ammeter and voltmeter. The AC resistance was computed by multiplying a constant value of 1.25 to the previously determined DC resistance. Table 2 displays the results of the DC resistance measurement findings. Temperature variation is neglected in the estimation of stator resistance.

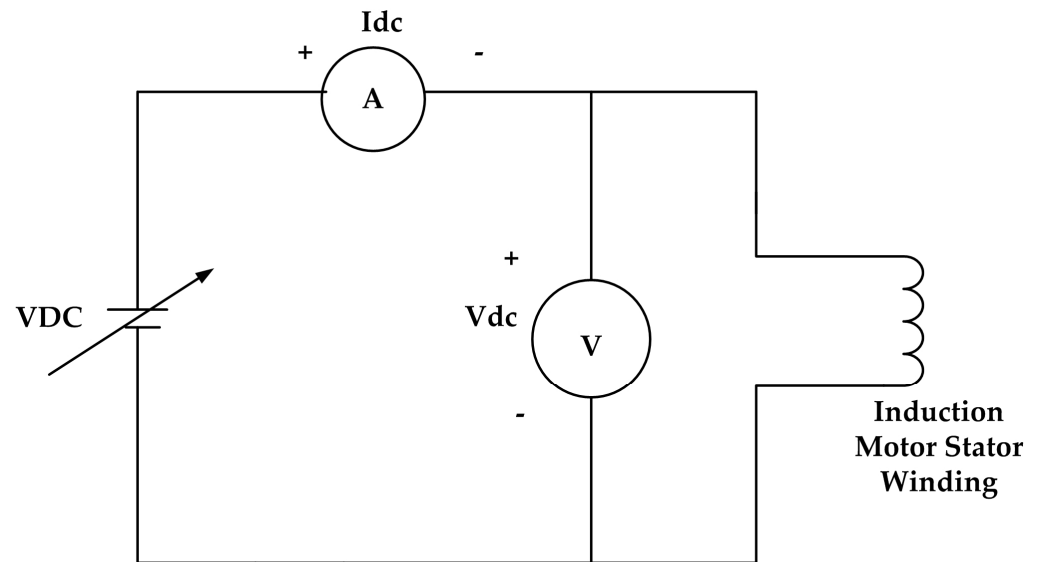


Figure 7. Estimation of stator winding DC resistance.

Table 2. Experimental observations on stator winding resistance estimation.

Sl No.	Applied Voltage (volt)	Current (amp)	DC Resistance (ohm)	Average dc Resistance (ohm)	Stator ac Resistance (ohm)
1	6.82	1.5	4.55		
2	9.34	2	4.67	4.57	5.71
3	11.21	2.5	4.484		

4.1.2. No-Load Test

The voltages at rated value and frequency are applied during the no-load test or light-load test. The circuit arrangement for the no-load test is shown in Figure 8. The input current, power input, and applied voltages are noted. As the input power factor is less than 0.5, low power factor watt meters are used, and one of the wattmeter shows a negative reading. Total power input corresponds to stator copper and iron losses without any applied load. No-load power factor, core loss resistance, magnetizing current, and inductances are determined from the measurements obtained. The observations obtained during no-load tests are presented in Table 3.

Table 3. Observations of No-Load Test.

Voltage V_{as} (volt)	I_a (amp)	I_b (amp)	I_c (amp)	No-Load Current I_o (amp)	W1 (watts)	W2 (watts)	Power Input P_{oc} (watts)	Speed (rpm)
415	4.15	4.1	4.1	4.12	-672	1080	408	1498

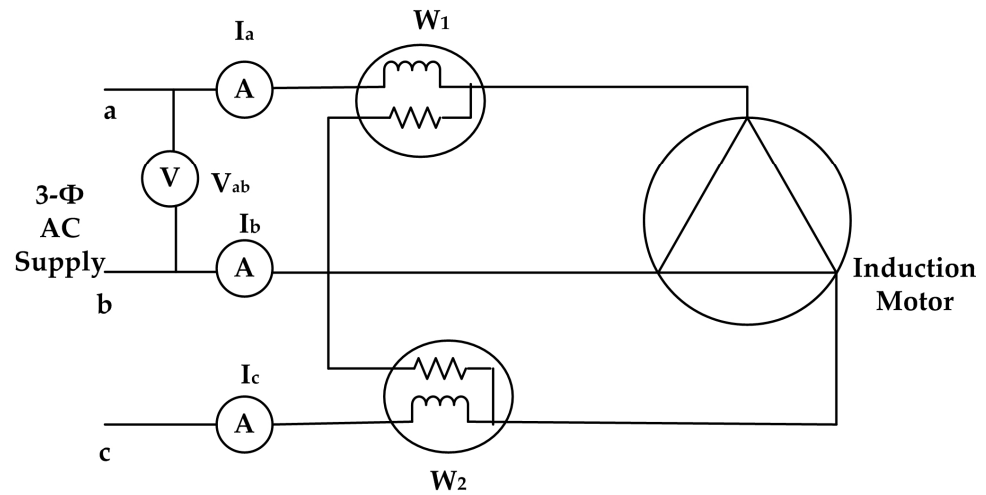


Figure 8. Circuit arrangement for no-load test.

4.1.3. Locked Rotor or Short Circuit Test

With locking the rotor to prevent rotation, applied voltage to the stator is increased until rated current flows to the stator. With the voltage, current, and power input readings obtained, rotor resistance and leakage inductance are calculated by developing the equivalent circuit. The results that were obtained from the examination are shown in Table 4.

Table 4. Locked rotor test observations.

SC Voltage V_{sc} (volt)	SC Current I_{sc} (Amp)	W1 (watts)	W2 (watts)	SC Power Input P_{sc} (watts)
82	7.5	-11	510	499

4.1.4. Locked Rotor or Short Circuit Test

The exact equivalent circuit (IEEE) model of an induction motor was built based on the findings made during the blocked rotor and no-load tests, as illustrated in Figure 9. Table 5 presents an estimation of the values for the machine parameters based on the results of the tests performed on the induction motor using the equivalent circuit model [49,50].

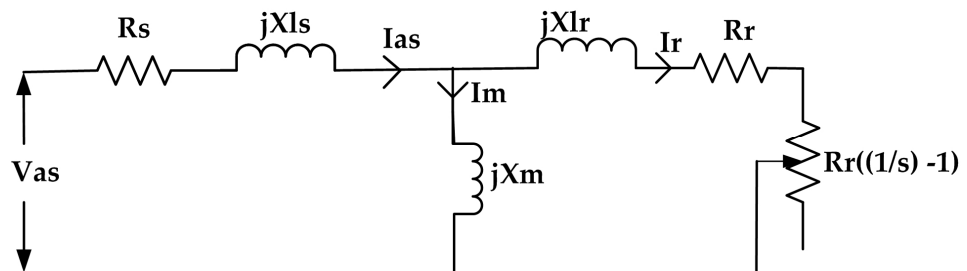


Figure 9. Exact circuit (IEEE) model of induction motor.

Table 5. Induction motor parameters obtained from DC test, no-load, and blocked rotor tests.

R_s (ohm)	R_r (ohm)	$L_s = (L_{ls} + L_m)$ (Henry)	$L_r = (L_{lr} + L_m)$ (Henry)	L_m (Henry)
5.7	4.11	0.5634	0.5634	0.5379

4.2. Modeling Analysis

The block diagram of the induction motor drive with integrated online rotor and stator resistance estimator with speed estimation is shown in Figure 10. The induction motor drive is operated with a rotor flux orientation controller. A multi-level low-pass filter is used for the estimation of voltage model fluxes from the measured stator voltages and currents [51,52]. The induction motor parameters are obtained from no-load and blocked rotor tests performed in the laboratory as presented in Section 4.1. Induction motor parameter details used in the simulation study are summarized in Table 6. Simulations are performed individually on the rotor resistance estimator, stator resistance estimator, and on an integrated system as shown in Figure 10. The performance of the developed algorithms is evaluated by simulation using MATLAB/Simulink software (R2023b, MathWorks, Natick, MA, USA).

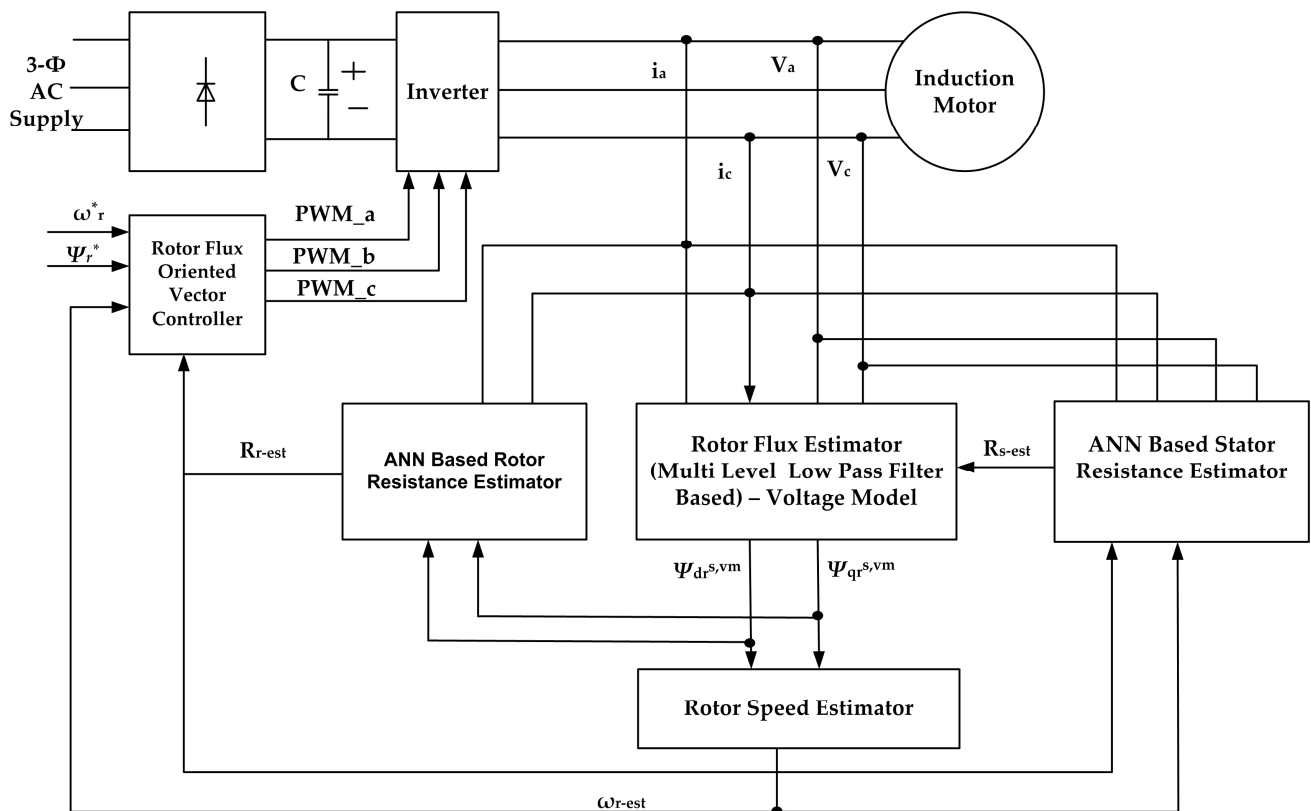


Figure 10. Block diagram of rotor-flux-oriented indirect vector-controlled induction motor drive with online rotor and stator resistance estimation.

The stator resistance, rotor resistance, and speed are estimated as presented in the following steps:

- With the sampled terminal voltages and currents and by using the developed neural network model as presented in Section 3, stator resistance is estimated online.
- Using the obtained stator resistance, rotor fluxes are estimated. Using the neural network model as presented in Section 2, rotor resistance is determined.
- The speed is evaluated by using the obtained stator resistance, rotor resistance, and rotor fluxes as presented in Section 3.

The results of the simulation are presented in the following sections.

Table 6. Induction motor parameter details.

Parameters	Values
Rated power	3.7 kW
Rated frequency	50 Hz
Rated voltage	415 V
Rated current	7.5 A
Number of poles	4
Type of stator connection	Delta
No-load speed	1498 rpm
Rotor resistance	4.11 Ohm
Stator resistance	5.7 Ohm
Rotor inductance (Lr)	0.5634 H
Stator inductance (Ls)	0.5634 H
Magnetizing inductance (Lm)	0.5379 H
Moment of inertia (Jr)	0.01542 kg-m ²

4.2.1. Simulation Results of the Performance of the Rotor Resistance Estimator and Analysis

The initial actual resistance values of rotor and stator windings were obtained from the various laboratory tests and are shown in Table 5. To evaluate the ability of the proposed algorithm to track the variation in the rotor resistance, the simulations were performed with the wide range of actual rotor and stator resistance values under the various conditions such as fixed stator resistance and speed, fixed stator resistance and varying speed, and varying stator resistance and speed. Simulations are performed by considering the actual rotor resistance values of 10, 15, 20, 25, 40, 50, 75, 90, and 100 percent step rises from its initial value under the condition of fixed stator resistance and speed. Also, arbitrarily stepped rises in rotor and stator resistance values are considered to evaluate the performance of the algorithm with both variable speed and stator resistance.

The training of the neural network is performed in all the above conditions with the parameters as presented in Table 7. These parameters are selected based on a trial-and-error process by performing repeated training trials.

Table 7. Training parameters of neural network for rotor resistance.

Parameter	Value
The initial learning rate for weight W_1	2.4×10^{-4}
The initial learning rate for weight W_3	10×10^{-6}
Steepness factor of bipolar sigmoid function s_1 and s_3	1
α_1, α_3	0.1
Sampling time T_s	2 ms

The simulation results (testing) are presented in Tables 8–10 and Figures 11–13. A stepped increase in the actual rotor resistance, speed, and stator resistance is presented for the simulation purpose to evaluate the performance which is not true under the actual operating conditions. The percentage estimation error in rotor resistance in each case is also shown.

The variation in learning rates, weight adjustment factors, resistance value, and convergence of squared error during the training of the neural network is shown in Figure 14. As the iteration progresses, the estimated error between the fluxes decreases, giving rise to an increase in learning rates for the succeeding iterations, followed by a larger rate of weight adjustment. This results in quicker convergence of the error to the acceptable minimum value. Thus, the adaptive learning rate results in a quick estimation of the resistance with minimal error. As the iteration progresses, the squared error decreases, reaches the minimum value, then again increases, as shown in Figure 14c. The iteration is stopped when the error converges to the minimum value.

Table 8. Estimated rotor resistance with percentage error in estimation and number of iterations for fixed stator resistance and speed.

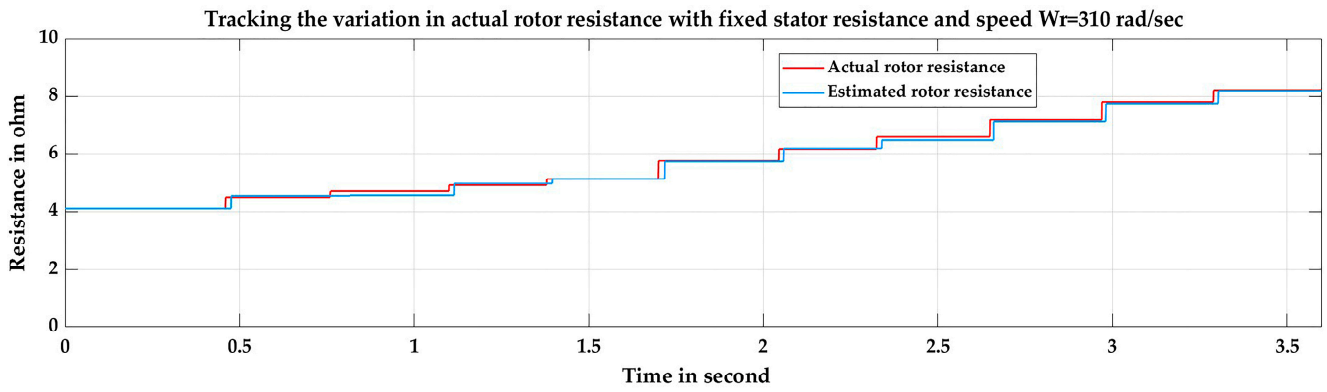
Actual Rotor Resistance	$W_r = 307$ Radian/Second			$W_r = 310$ Radian/Second		
	Estimated Resistance	Percentage Error	Number of Iterations	Estimated Resistance	Percentage Error	Number of Iterations
4.11	4.11	0	1	4.11	0	1
4.521	4.54	-0.4242	6	4.568	-1.033	6
4.7265	4.761	-0.7391	8	4.59	3.36	6
4.932	4.954	-0.4538	10	4.982	-1.01	9
5.1375	4.995	2.765	10	5.141	-0.06854	10
5.754	5.631	2.14	14	5.736	0.3159	13
6.165	6.335	-2.754	9	6.188	-0.3811	15
6.576	6.642	-1.008	10	6.464	1.709	16
7.1925	7.154	0.5389	12	7.129	0.8871	18
7.809	7.826	-0.219	16	7.756	0.68	19
8.22	8.345	-1.525	17	8.194	0.3145	20

Table 9. Estimated rotor resistance with percentage error in estimation and number of iterations for fixed stator resistance and varying speed.

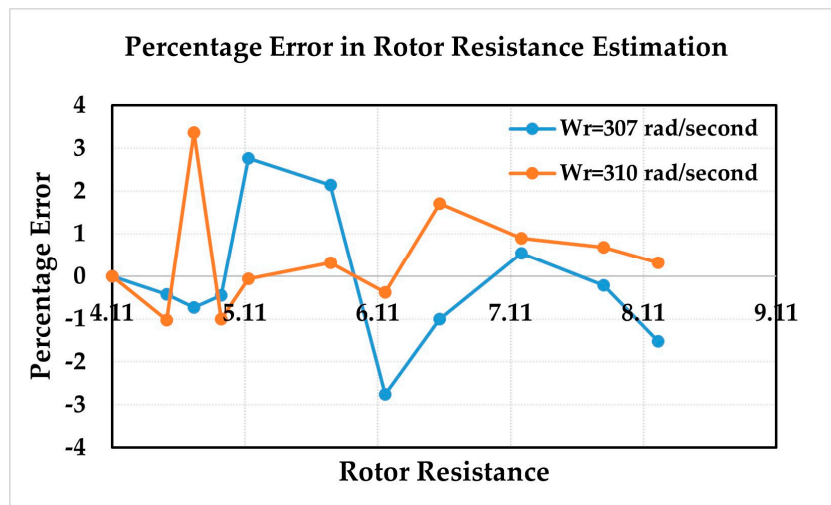
Actual Rotor Resistance	Speed W_r (rad/s)	Estimated Rotor Resistance	Percentage Error	Number of Iterations
4.11	313	4.11	0	1
4.521	312	4.476	0.9889	5
4.7265	311	4.705	0.4627	7
4.932	310	4.958	-0.5192	9
5.137	309	5.072	1.283	10
5.754	308	5.661	1.62	14
6.165	308	6.08	1.385	16

Table 10. Estimated rotor resistance with percentage error in estimation and number of iterations for varying stator resistance and speed.

Actual Rotor Resistance	Actual Stator Resistance	Speed (rad/s)	Estimated Resistance	Percentage Error	Number of Iterations
4.11	5.7	313	4.11	0	1
4.521	6.27	312	4.472	1.077	5
4.726	6.55	311	4.812	-1.817	8
4.932	6.84	310	4.95	-0.3642	9
5.137	7.125	309	5.165	-0.5305	11
5.754	7.98	308	5.537	3.78	14
6.165	8.55	308	6.06	1.705	17

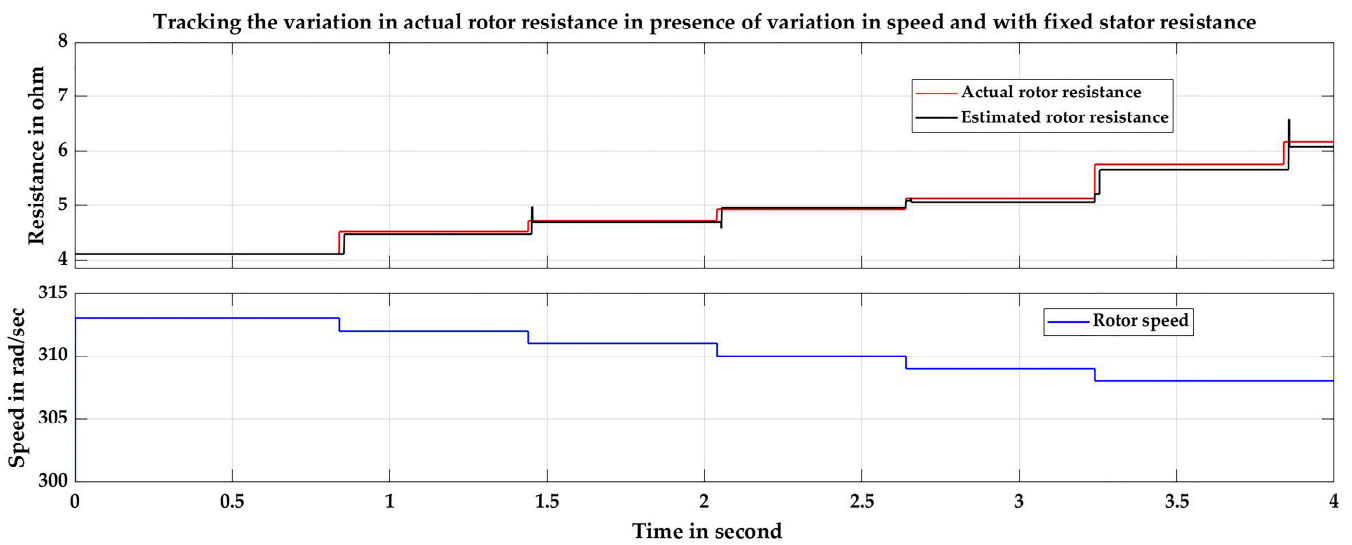


(a)



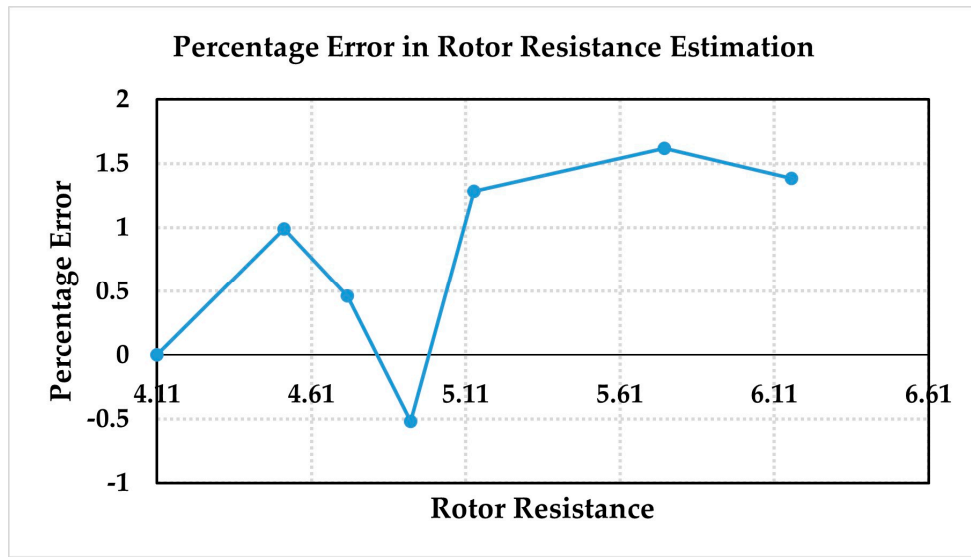
(b)

Figure 11. (a) Tracking the variation in actual rotor resistance with fixed stator resistance and speed at $W_r = 310$ radian/second. (b) Percentage error in rotor resistance estimation.



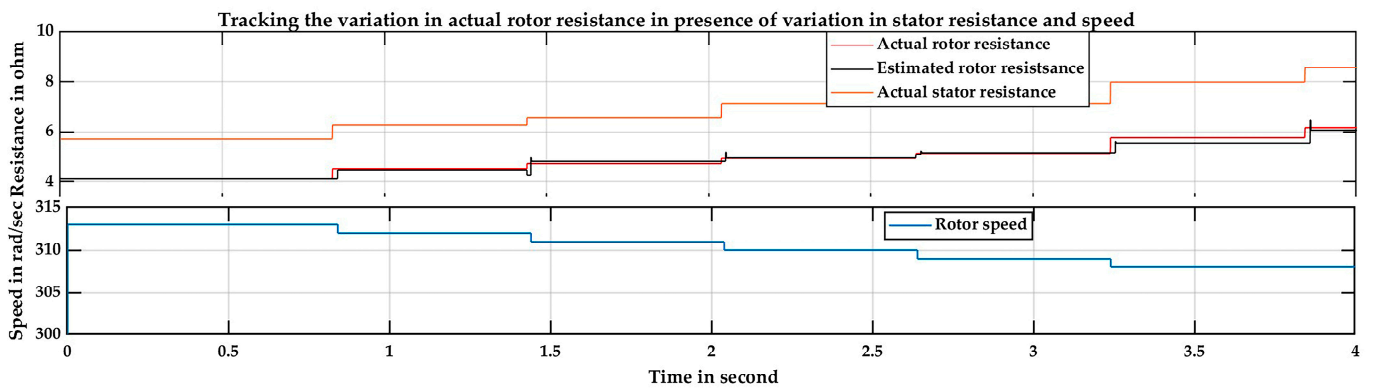
(a)

Figure 12. Cont.

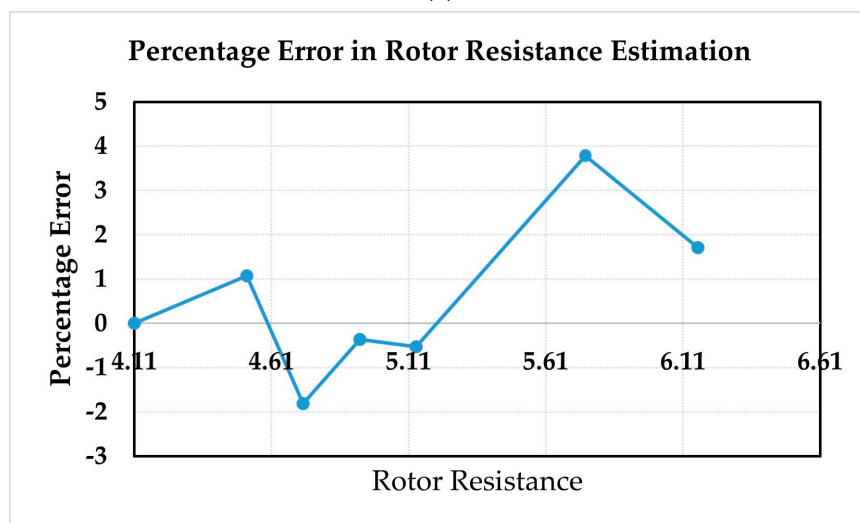


(b)

Figure 12. (a) Tracking the variation in actual rotor resistance with fixed stator resistance and at varying speeds. (b) Percentage error in rotor resistance estimation.



(a)



(b)

Figure 13. (a) Tracking the variation in actual rotor resistance with varying stator resistance and varying speed. (b) Percentage error in rotor resistance estimation.

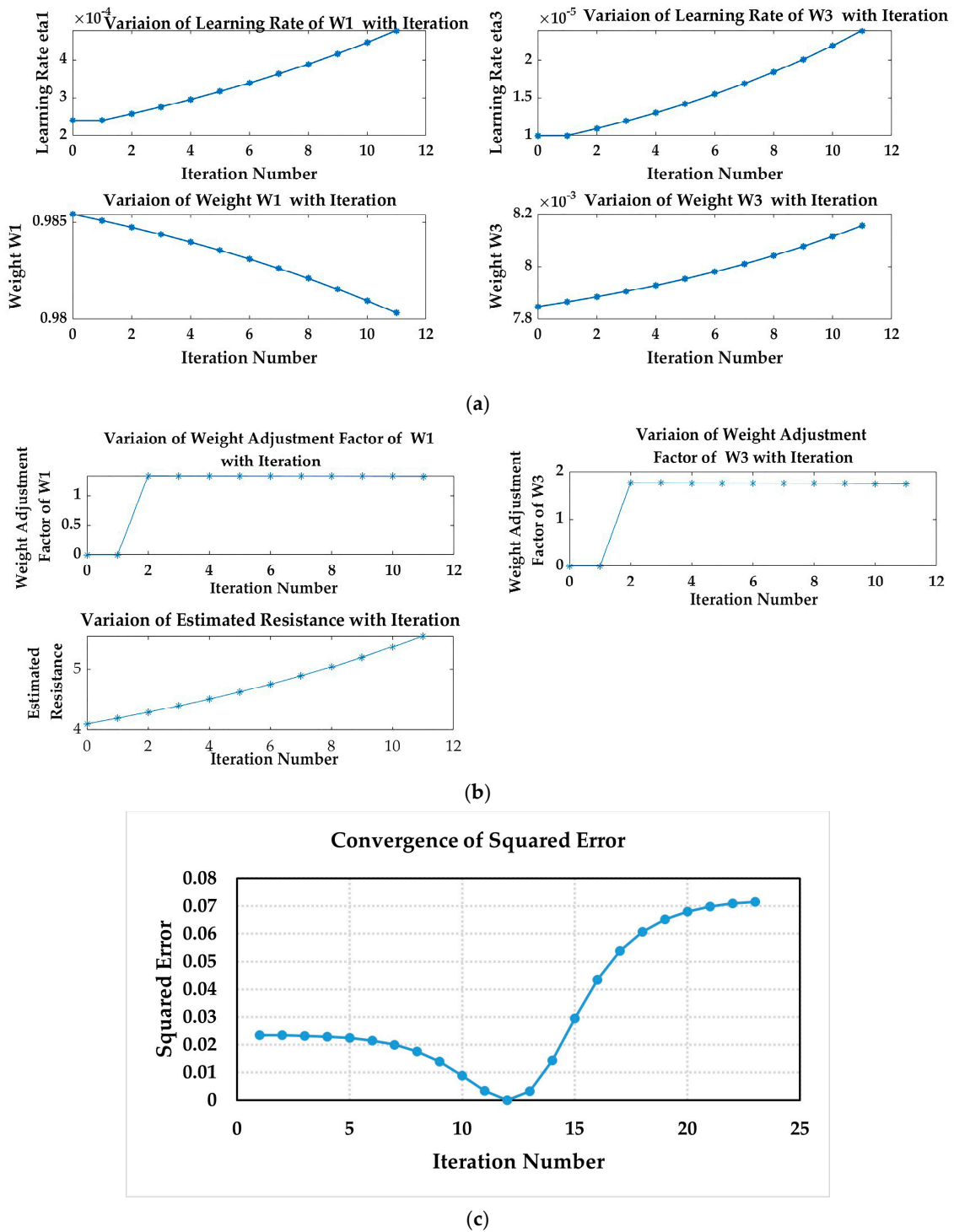


Figure 14. (a) Variation in learning rates, weights. (b) Weight adjustment factors, and resistance during the training. (c) Variation of squared error during network training.

4.2.2. Simulation Results of Performance of Stator Resistance Estimator and Analysis

The performance of the proposed back-propagated recurrent neural network with a bipolar sigmoid-based adaptive learning rate algorithm for tracking the variation in stator resistance is evaluated for 10, 15, 20, 25, 40, 50, 75, 90, and 100 percent rises from its nominal value under the various conditions as with fixed rotor resistance and speed, fixed rotor resistance and variable speed, and variable speed and rotor resistance. The training of the neural network is performed in all the above conditions with the parameters as presented

in Table 11. These parameters are selected based on a trial-and-error process by performing repeated training trials.

Table 11. Training parameters of neural network for stator resistance.

Parameter	Value
The initial learning rate for weight W_4	0.001
Steepness factor of bipolar sigmoid function s_4	0.01
α_4	4
Sampling time T_s	4 ms

The simulation results are presented in Tables 12–14 and Figures 15–17. A stepped increase in the actual rotor resistance, speed, and stator resistance is presented for the simulation purpose to evaluate the performance which is not true under the actual operating conditions.

Table 12. Estimated stator resistance with percentage error in estimation and number of iterations for fixed rotor resistance and speed.

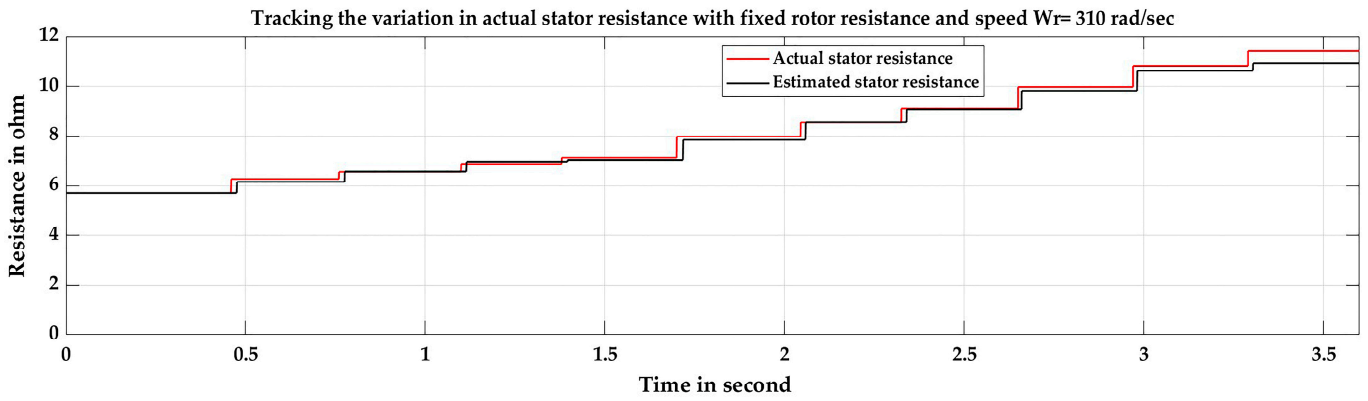
Actual Stator Resistance	$W_r = 307 \text{ rad/s}$			$W_r = 310 \text{ rad/s}$		
	Estimated Resistance	Percentage Error	Number of Iterations	Estimated Resistance	Percentage Error	Number of Iterations
5.7	5.7	0	1	5.7	0	1
6.27	6.325	−0.8841	5	6.154	1.857	6
6.55	6.519	0.4765	7	6.561	−0.1756	8
6.84	6.742	1.437	7	6.926	−1.25	10
7.125	6.994	1.838	8	6.99	1.901	10
7.98	7.932	0.6067	11	7.838	1.778	13
8.55	8.415	1.578	12	8.558	−0.091	15
9.12	8.955	1.807	13	9.091	0.3181	16
9.975	9.684	2.916	15	9.819	1.566	17
10.83	10.5	3.068	16	10.63	1.848	18
11.4	10.79	5.366	16	10.94	4.078	19

Table 13. Estimated stator resistance with percentage error in estimation and number of iterations for fixed rotor resistance and varying speed.

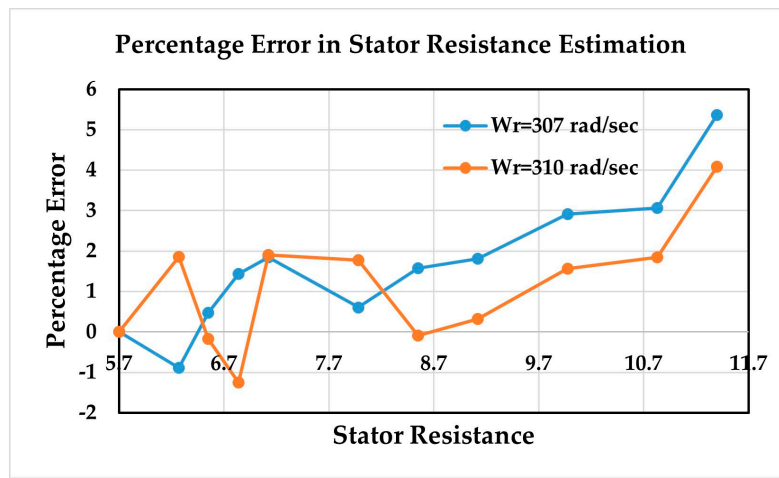
Actual Stator Resistance	Speed W_r (rad/s)	Estimated Stator Resistance	Percentage Error	Number of Iterations
5.7	313	5.7	0	1
6.27	312	6.307	−0.5941	8
6.55	311	6.615	−0.9972	9
6.84	310	6.92	−1.166	10
7.125	309	7.085	0.566	11
7.98	308	7.956	0.3065	12

Table 14. Estimated stator resistance with percentage error in estimation and number of iterations for varying rotor resistance and speed.

Actual Stator Resistance	Actual Rotor Resistance	Speed W_r (rad/s)	Estimated Stator Resistance	Percentage Error	Number of Iterations
5.7	4.11	313	5.7	0	1
6.27	4.727	312	6.306	−0.5775	6
6.55	5.138	311	6.616	−1.009	11
6.84	5.343	310	6.74	1.456	10
7.685	5.548	309	7.633	0.6825	14
8.55	6.165	308	8.18	4.21	14

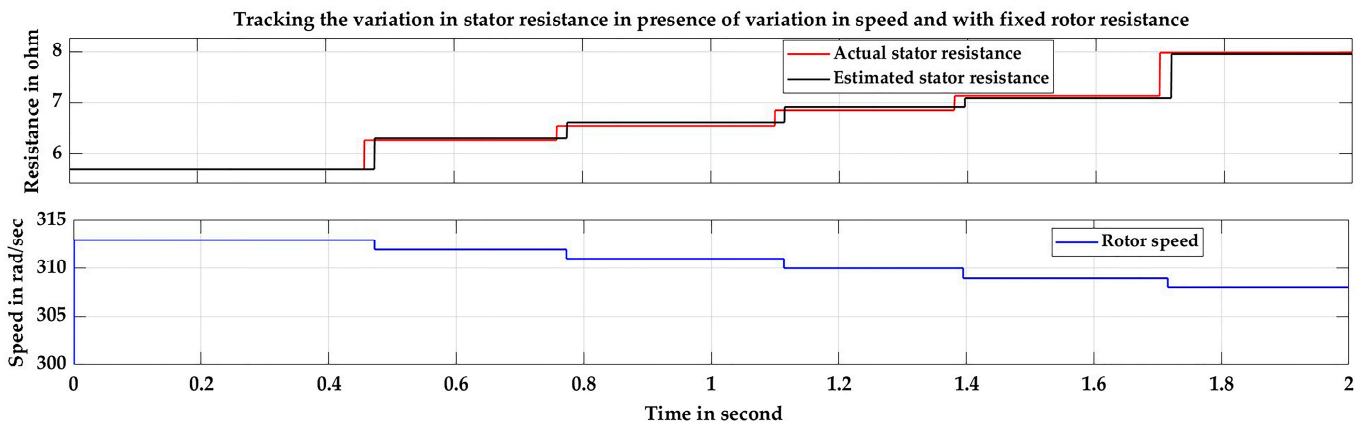


(a)



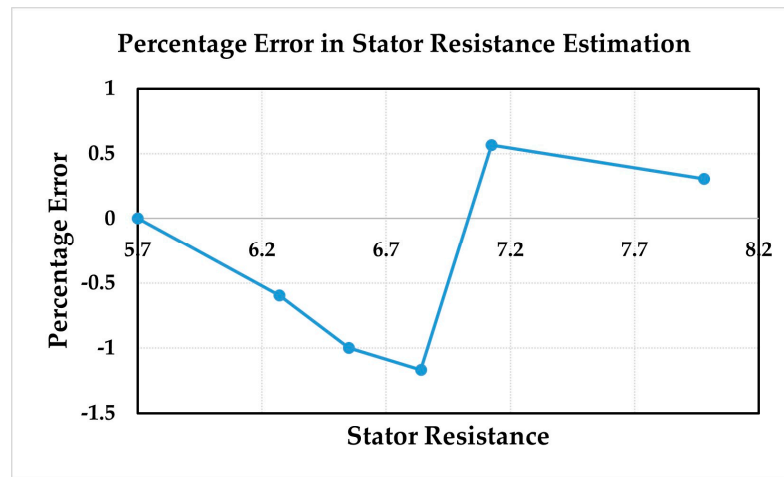
(b)

Figure 15. (a) Tracking the variation in actual stator resistance with fixed rotor resistance and speed at $W_r = 310$ rad/s, (b) Percentage error in stator resistance estimation.



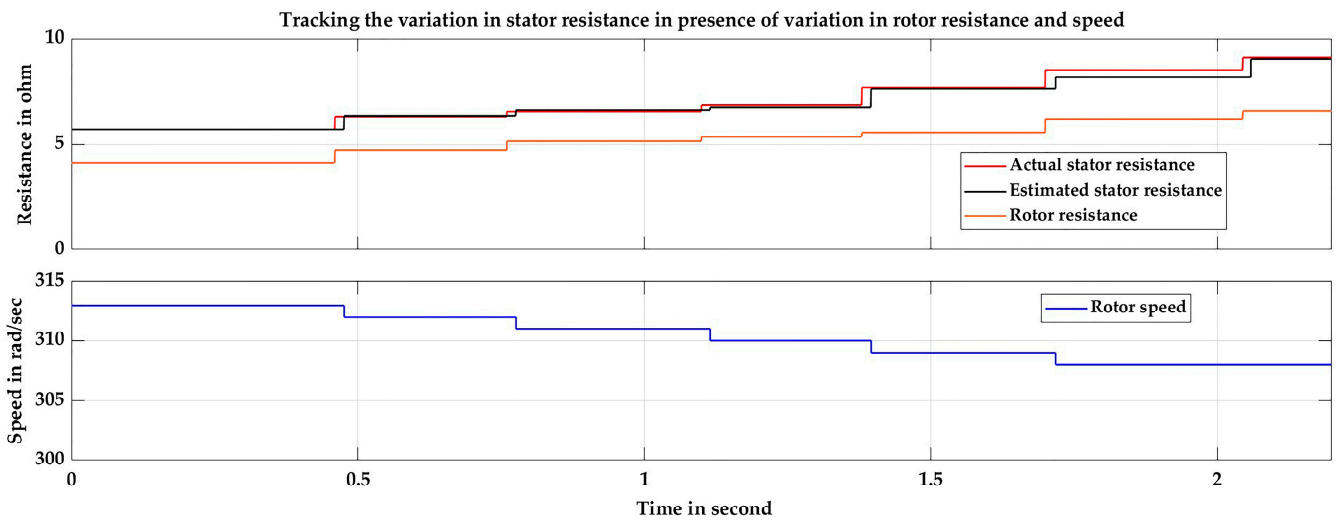
(a)

Figure 16. Cont.

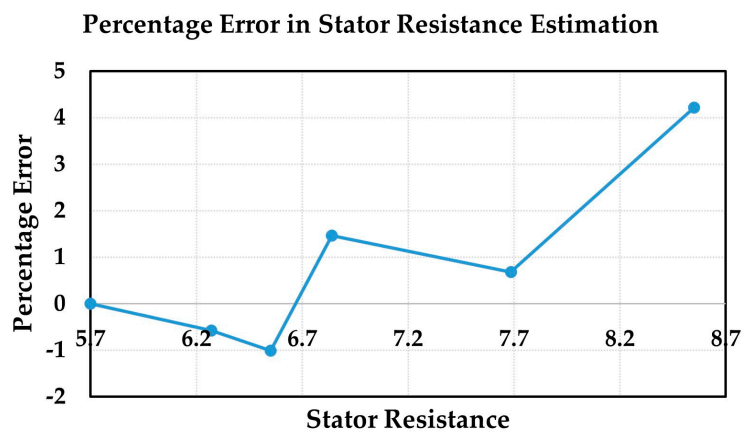


(b)

Figure 16. (a) Tracking the variation in actual stator resistance with fixed rotor resistance and at varying speeds. (b) Percentage error in stator resistance estimation.



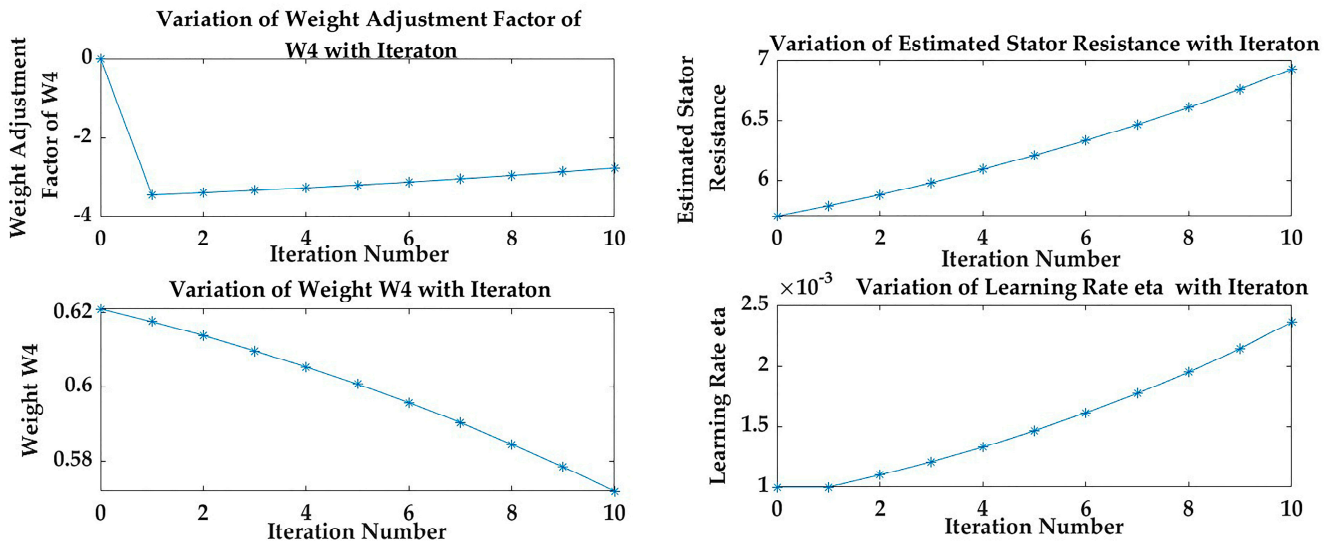
(a)



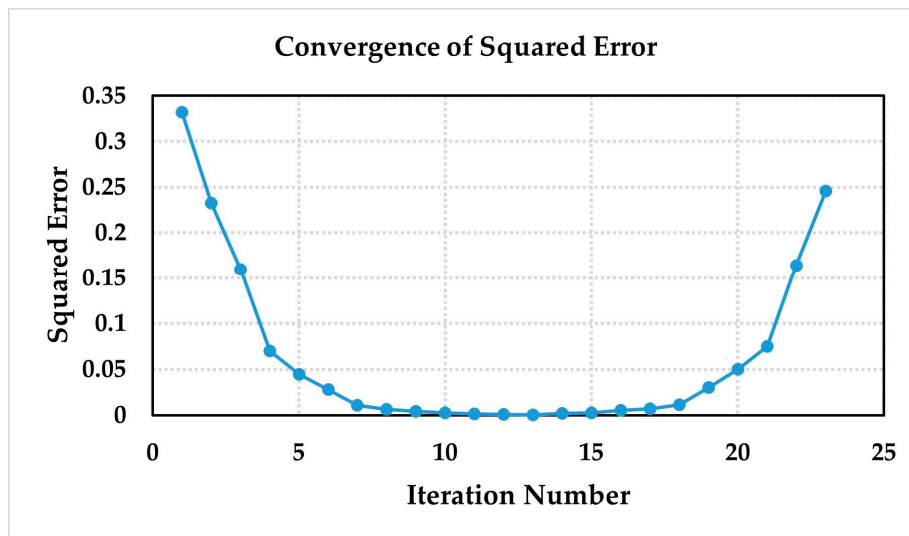
(b)

Figure 17. (a) Tracking the variation in actual stator resistance with varying rotor resistance and varying speed. (b) Percentage error in stator resistance estimation.

As the iteration progresses during the training, the learning rate increases due to the decrease in error between the actual stator current and the estimated current from the neural current model, leading to weight adjustments at a larger rate in the succeeding iterations. Hence, quicker convergence of the error to an acceptable value is obtained, as presented in Figure 18a. As the iteration progresses, squared error falls initially, converges to minimum value, and then increases, as shown in Figure 18b.



(a)



(b)

Figure 18. (a) Variation in learning rates, weights, weight adjustment factors, and resistance during the training. (b) Convergence of squared error.

4.2.3. Speed Estimation with Integrated Online Rotor and Stator Resistance Estimation

The simulation results of the integrated system are shown in Figure 19. The online rotor and stator resistance estimator tracks the variation in the rotor and stator resistance precisely with minor errors. With online rotor and stator resistance estimation, actual drive speed is measured accurately, which closely follows the set reference speed within the error of 0.16%.

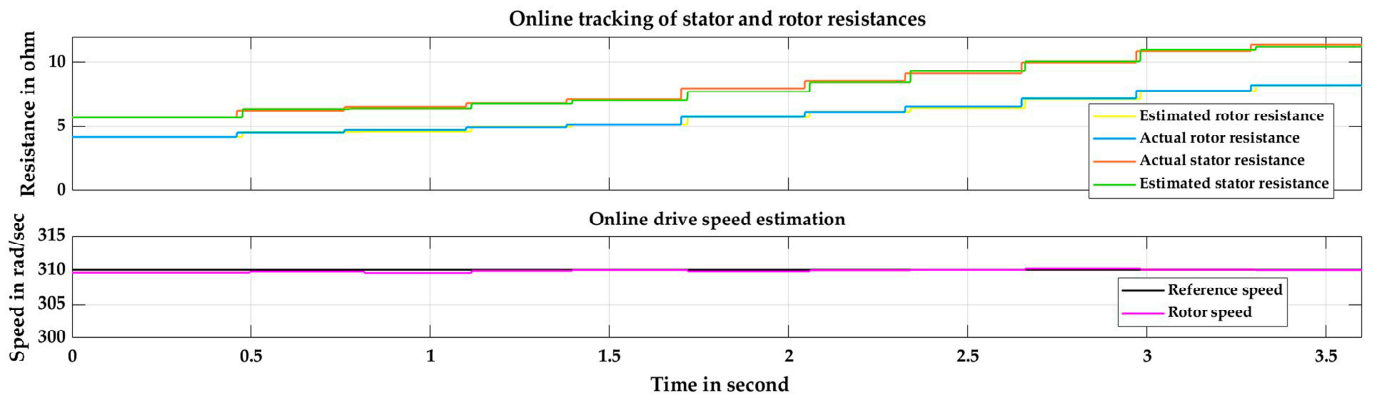


Figure 19. Online rotor and stator resistance estimation along with speed estimation.

4.3. Experimental Evaluation and Results

The proposed rotor and stator resistance, together with the speed estimation algorithm, was verified on an induction motor drive with a rotor flux orientation scheme [49], as shown in Figures 20 and 21. The DSpace DS1104 controller board residing in the PC is employed for experimenting. The experiment is performed on a 3-phase induction motor with the rating as detailed in Table 6. The induction motor is driven with an IGBT inverter operated with a 5 kHz switching frequency. The induction motor is loaded through a rigidly coupled DC motor of 3 kW for torque control with the help of a 4Q rectifier. The proposed stator and rotor resistance estimation blocks are implemented with a sampling time of 2000 μ s; a sampling time of 200 μ s is employed for current and flux controllers and a 2000 μ s sampling time for the speed estimator. For position and speed feedback, an encoder with 5000 pulses/cycles is used.

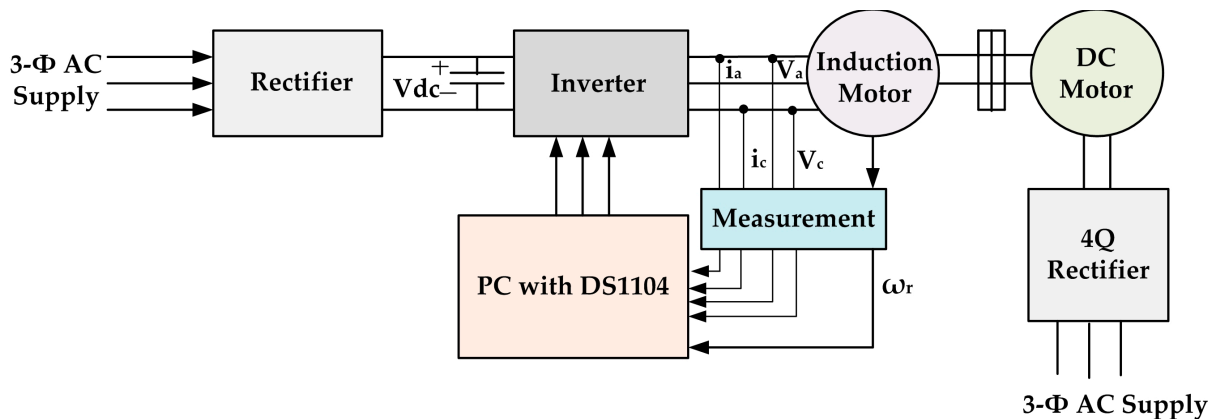
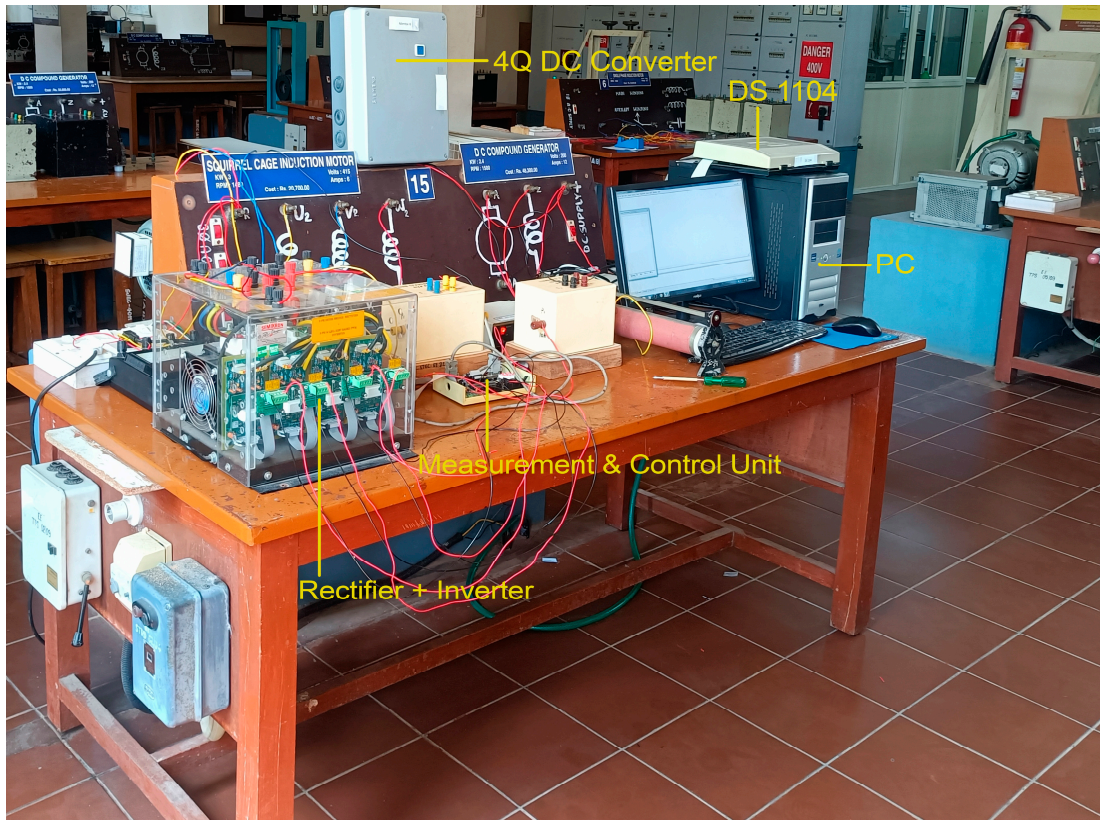
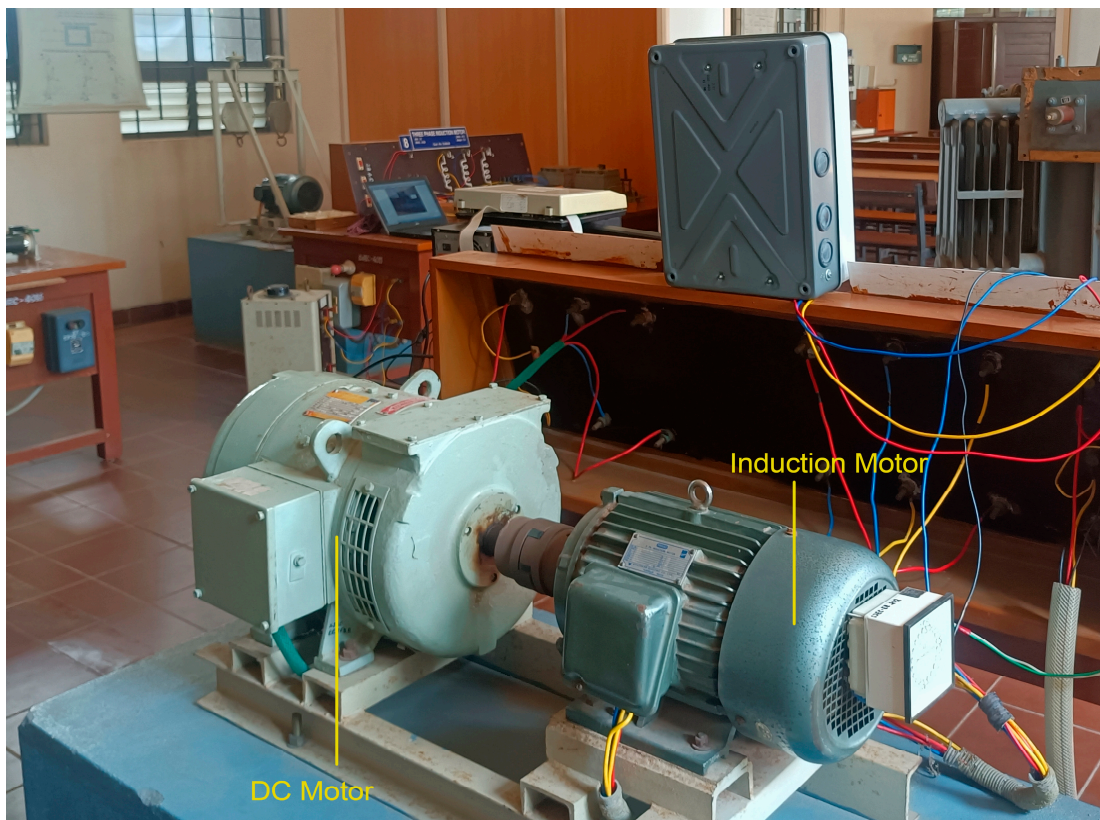


Figure 20. Block diagram of the experimental setup.

The ability of the proposed rotor resistance estimator to track the actual rotor resistance is evaluated by conducting the temperature rise test at an ambient temperature of 25 $^{\circ}$ C, where the motor is loaded with 6.4 N-m and driven at 1480 rpm. The results obtained for the estimated stator and rotor resistances collected from the experiment for nearly an hour are presented in Figure 22. As the motor runs with the load, the temperature of the stator and rotor winding rises, leading to a rise in resistance values. The d-axis rotor flux linkages collected from the voltage model and neural network model at the end of the heat run test are presented in Figure 23. The estimated d-axis rotor flux by the neural network model precisely tracks that of the voltage model and current model within an error of 1.2%.

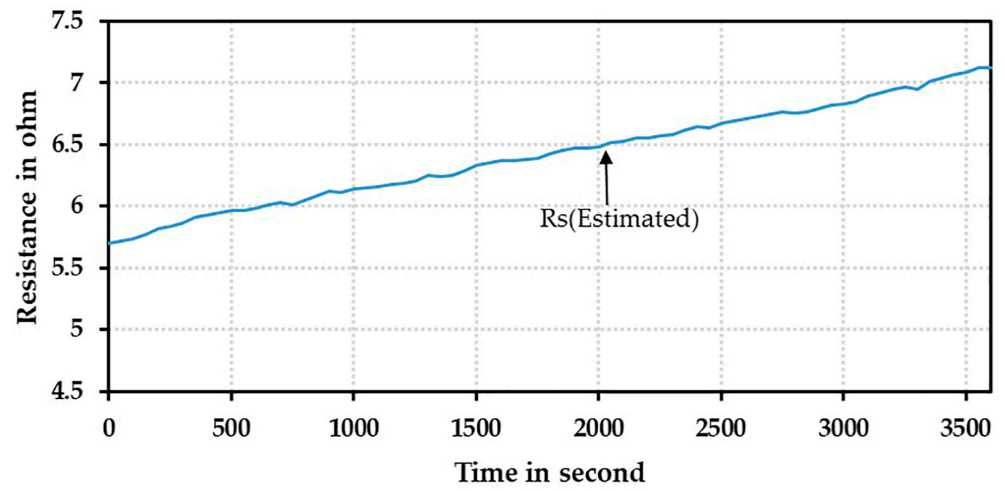


(a)

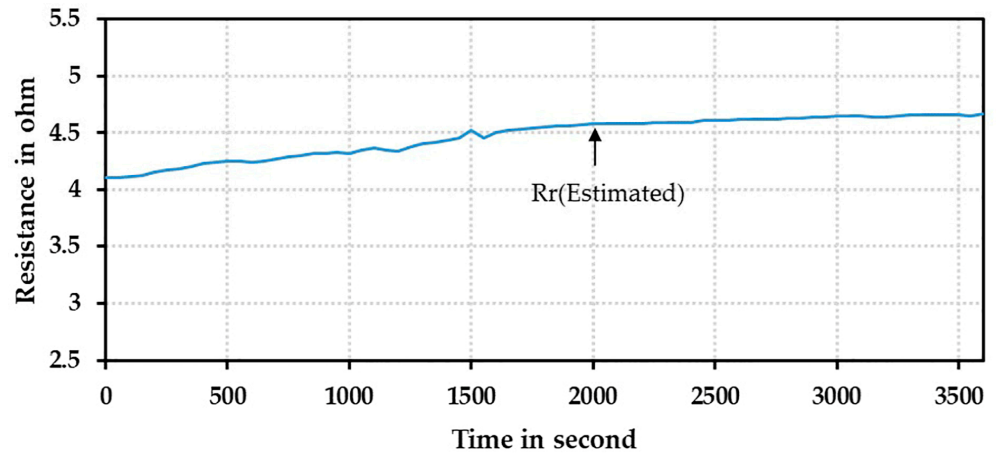


(b)

Figure 21. (a) Test bench I setup. (b) Motor-load setup.



(a)



(b)

Figure 22. Experimentally estimated (a) stator and (b) rotor resistances.

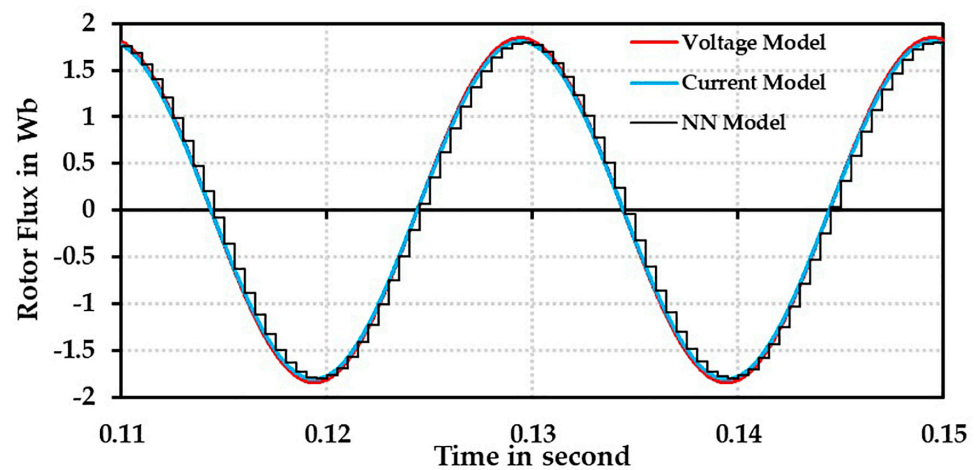


Figure 23. Experimentally estimated rotor flux at the end of temperature run test.

The performance of the stator resistance estimator is evaluated by adding a resistance of 2.8 ohms per phase in series with the stator windings of the induction motor. The addition of 2.8 ohm raises the stator resistance value from 5.7 ohm to 8.5 ohm, as shown in Figure 24. A torque of 6.4 Nm was applied with the motor running at 1480 rev/min. The estimated stator resistance tracks the actual stator resistance precisely and converges closely

to 8.46 ohm with an error of 0.48%, as shown in Figure 24 with the proposed adaptive learning rate algorithm. With the conventional constant rate learning algorithm, an error of 1.9% is obtained on stator resistance estimation. With the proposed adaptive learning rate algorithm, the stator resistance estimation converges within 150 ms as compared to the conventional constant learning rate algorithm of around 250 ms. A pulsation of 0.35% is obtained in stator resistance estimation with the proposed algorithm as against 1.56% with the conventional constant learning rate approach.

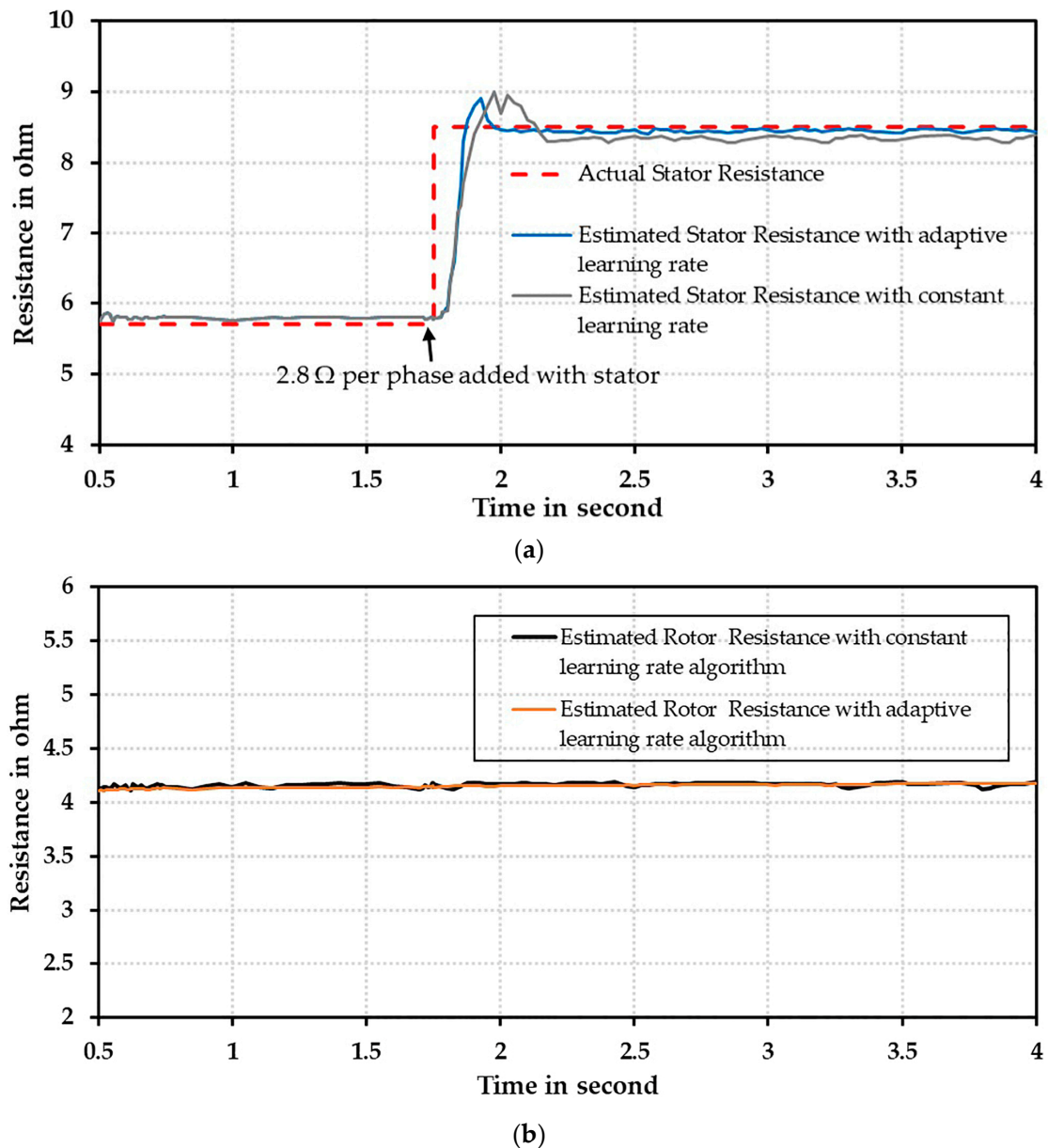


Figure 24. Tracking the actual (a) stator and (b) rotor resistance in the experiment by the conventional constant learning rate and adaptive learning rate algorithms.

The tracking of the d-axis stator current by the neural network model during the online estimation of the stator resistance is shown in Figure 25. The estimated current by the neural network model closely follows the d-axis measured stator current owing to the online training of the neural network.

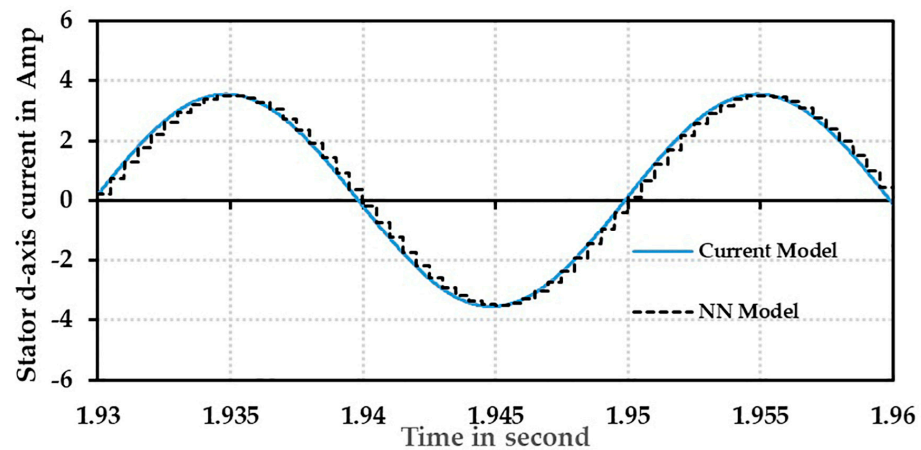


Figure 25. Measured stator d-axis current and obtained from neural network model during stator resistance estimation.

The results obtained for stator resistance estimation from the experiment are compared with the developed model by applying a step change in stator resistance of 2.8 ohms without making any changes in R_r . The simulation is carried out simultaneously with the conventional and the proposed adaptive learning rate algorithm. The results obtained from the model simulation, as shown in Figure 26, show close agreement with the experimental results shown in Figure 24. With the proposed adaptive learning rate algorithm, the estimated resistance converges at 8.53 ohm with an error of -0.35% , whereas, with the conventional constant learning rate algorithm, the estimated stator resistance converges at 8.624 ohms with an error in the estimation of -1.46% .

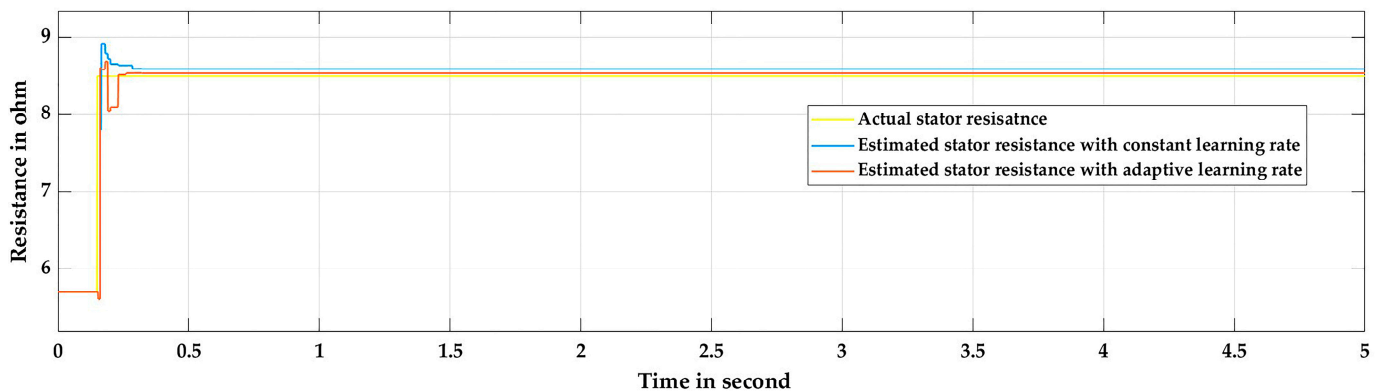


Figure 26. Simulation results of tracking the stator resistance by the conventional and proposed adaptive learning rate algorithms.

The experiments were performed to evaluate the performance of the proposed stator and rotor estimator along with the speed sensorless operation. To evaluate the effect of variation in the stator resistance on the speed estimation, a 2.8 ohm resistance per phase is added to the stator windings. The addition of 2.8 ohm raises stator resistance from its nominal value of 5.7 ohm to 8.5 ohm. The drive is operated with RFOC. When the stator resistance estimator block is off, the speed drops to 1472 rpm, as shown in Figure 27. With the stator resistance estimator block on, the estimated speed was closely matching with the measured speed.

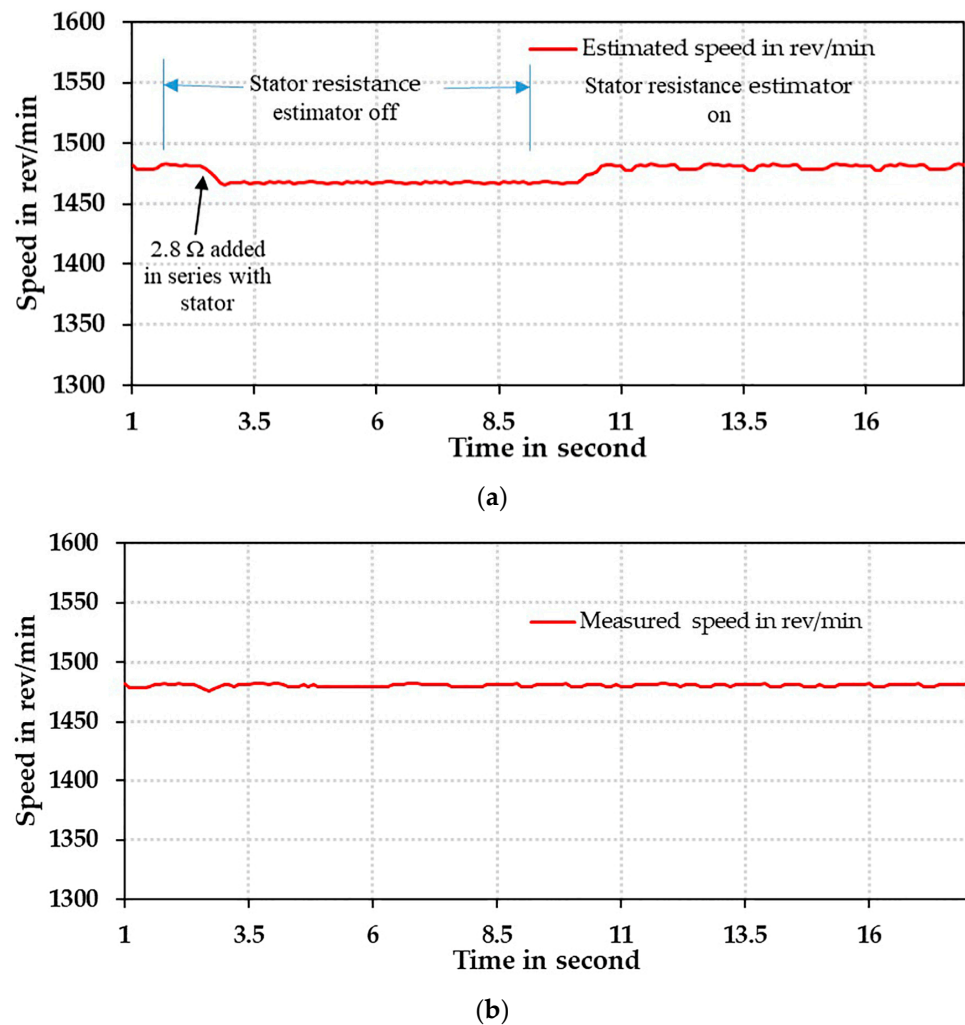


Figure 27. Experimental results showing the effect of stator resistance estimation on (a) dynamic speed estimation and (b) measured speed.

4.4. Discussion

The results of the simulations and hardware, as presented in the preceding sections, point out that

- As the number of iterations needed for the estimation of stator and rotor resistances is reduced with the proposed algorithm, the quick estimation of stator and rotor resistances is obtained as compared to the conventional constant learning rate approach. For the step change in the stator resistance, with the proposed approach, estimated stator resistance converges with the minimum error of estimation within 150 ms as compared to 250 ms obtained from the conventional constant learning rate approach [7].
- The proposed algorithm ensures the reduction in error of estimated resistances. For the step change in stator resistance, with the proposed approach, the estimation error is 0.48%, which is superior to the conventional constant learning rate approach of around 2%.
- The proposed algorithm tracks the stator resistance smoothly with the pulsation in estimated resistance within 0.35%, which is better than the constant learning rate or other function-based learning rate approach [8].
- The smooth estimation of speed is obtained with the developed algorithm where pulsation is within 0.4% which is much lower than that obtained by a conventional constant learning rate algorithm [24].

5. Conclusions

This paper presents an advanced back-propagation neural network with error-function-based adaptive learning rate algorithms for the online estimation of stator and rotor resistances used in speed sensorless vector-controlled IMD. As compared with the constant learning rate, the suggested back-propagation algorithm for the feed-forward network performs superiorly with an adjustable learning rate defined by a bipolar sigmoid function. The results of the simulation and hardware experiments justify the ability of the proposed algorithm to track the variation in stator and rotor resistances quickly and precisely, leading to the estimation of the speed close to the real speed. The proposed algorithm has the potential to improve the control quality of the vector-controlled speed sensorless IMD. Further, the developed algorithm could be used to evaluate the drive's performance in different operating states.

Author Contributions: Conceptualization, A.K.M.K. and R.B.I.; methodology, A.K.M.K. and S.S.; software, S.B.J. and A.B.S.; validation, A.K.M.K., R.B.I., S.B.J. and S.S.; formal analysis, A.K.M.K.; investigation, A.K.M.K.; resources, A.K.M.K. and R.B.I.; data curation, A.K.M.K.; writing—original draft preparation, A.K.M.K.; writing—review and editing, A.K.M.K.; visualization, A.K.M.K.; supervision, R.B.I.; project administration, R.B.I. All authors have read and agreed to the published version of the manuscript.

Funding: This research received no external funding.

Data Availability Statement: The original contributions presented in the study are included in the article, further inquiries can be directed to the corresponding author.

Acknowledgments: The authors would like to place on record their sincere gratitude to all individuals directly or indirectly involved in this experimental research and preparation of this manuscript. Special thanks to St. Joseph Engineering College and Visvesvaraya Technological University.

Conflicts of Interest: The authors declare no conflicts of interest.

List of Symbols

$\psi_{dr}^{s,vm}$	Voltage model d -axis rotor flux linkages in the stator reference frame
$\psi_{qr}^{s,vm}$	Voltage model q -axis rotor flux linkages in the stator reference frame
i_{ds}^s	d -axis stator current in the stator reference frame
i_{qs}^s	q -axis stator current in the stator reference frame
v_{ds}^s	d -axis stator voltage in the stator reference frame
v_{qs}^s	q -axis stator voltage in the stator reference frame
$\psi_{dr}^{s,mm}$	Neural network model d -axis rotor flux linkages in the stator reference frame
$\psi_{qr}^{s,mm}$	Neural network model q -axis rotor flux linkages in the stator reference frame
$\psi_{dr}^{s,im}$	Induction motor current model d -axis rotor flux linkages in the stator reference frame
$\psi_{qr}^{s,im}$	Induction motor current model q -axis rotor flux linkages in the stator reference frame
R_s	Stator resistance
R_r	Rotor resistance
L_s	Stator self-inductance
L_r	Rotor self-inductance
L_m	Magnetizing inductance

References

1. Dianov, A.; Anuchin, A. Offline Measurement of Stator Resistance and Inverter Voltage Drop Using Least Squares. *IEEE Access* **2023**, *11*, 17053–17065. [[CrossRef](#)]
2. Dinolova, P.; Ruseva, V.; Dinolov, O. Energy Efficiency of Induction Motor Drives: State of the Art, Analysis and Recommendations. *Energies* **2023**, *16*, 7136. [[CrossRef](#)]
3. Montano, J.; Garzón, O.D.; Herrera-Jaramillo, D.A.; Montoya, O.D.; Andrade, F.; Tobon, A. Estimating the Parameters of a Three-Phase Induction Motor Using the Vortex Search Algorithm. *Iran. J. Sci. Technol. Trans. Electr. Eng.* **2024**, *48*, 337–347. [[CrossRef](#)]
4. Abbasi, M.A.; Bin Husain, A.R. Model Predictive Control of a Dual Induction Motor Drive Fed by a Single Voltage Source Inverter. *Turk. J. Electr. Eng. Comput. Sci.* **2018**, *26*, 1623–1637. [[CrossRef](#)]

5. Çanakoglu, A.I.; Yetgin, A.G.; Temurtaş, H.; Turan, M. Induction Motor Parameter Estimation Using Metaheuristic Methods. *Turk. J. Electr. Eng. Comput. Sci.* **2014**, *22*, 1177–1192. [[CrossRef](#)]
6. Jisha, L.K.; Thomas, A.A.P. A Comparative Study on Scalar and Vector Control of Induction Motor Drives. In Proceedings of the 2013 International Conference on Circuits, Controls and Communications (CCUBE), Bengaluru, India, 27–28 December 2013; IEEE: Piscataway, NJ, USA, 2013.
7. Karanayil, B.; Rahman, M.F.; Grantham, C. Online Stator and Rotor Resistance Estimation Scheme Using Artificial Neural Networks for Vector Controlled Speed Sensorless Induction Motor Drive. *IEEE Trans. Ind. Electron.* **2007**, *54*, 167–176. [[CrossRef](#)]
8. Van, T.P.; Tien, D.V.; Leonowicz, Z.; Jasinski, M.; Sikorski, T.; Chakrabarti, P. Online Rotor and Stator Resistance Estimation Based on Artificial Neural Network Applied in Sensorless Induction Motor Drive. *Energies* **2020**, *13*, 4946. [[CrossRef](#)]
9. Kim, Y.-R.; Sul, S.-K.; Park, M.-H. Speed Sensorless Vector Control of Induction Motor Using Extended Kalman Filter. *IEEE Trans. Ind. Appl.* **1994**, *30*, 1225–1233. [[CrossRef](#)]
10. Noori, O.B.; Mustafa, M.O. Flux and Speed Estimation of Induction Motors Using Extended Kalman Filter. *Int. J. Comput. Appl.* **2018**, *181*, 975–8887.
11. Moaveni, B.; Masoumi, Z.; Rahmani, P. Introducing Improved Iterated Extended Kalman Filter (IIEKF) to Estimate the Rotor Rotational Speed, Rotor and Stator Resistances of Induction Motors. *IEEE Access* **2023**, *11*, 17584–17593. [[CrossRef](#)]
12. Horváth, K.; Kuslits, M. Dynamic Performance of Estimator-Based Speed Sensorless Control of Induction Machines Using Extended and Unscented Kalman Filters. *Power Electron. Drives* **2018**, *3*, 129–144. [[CrossRef](#)]
13. Strandt, A.R.; Strandt, A.P.; Schneider, S.C.; Yaz, E.E. Stator Resistance Estimation Using Adaptive Estimation via a Bank of Kalman Filters. In Proceedings of the 2018 Annual American Control Conference (ACC), Milwaukee, WI, USA, 27–29 June 2018; IEEE: Piscataway, NJ, USA, 2018; pp. 1078–1083.
14. Karthikeyan, A.; Prabhakaran, K.K.; Nagamani, C. Stator Flux Based MRAS Speed and Stator Resistance Estimator for Sensorless PMSM Drive. In Proceedings of the 2017 14th IEEE India Council International Conference (INDICON), Roorkee, India, 15–17 December 2017; IEEE: Piscataway, NJ, USA, 2017; pp. 1–6.
15. Hasanzadeh, A.; Reed, D.M.; Hofmann, H.F. Rotor Resistance Estimation for Induction Machines Using Carrier Signal Injection With Minimized Torque Ripple. *IEEE Trans. Energy Convers.* **2019**, *34*, 942–951. [[CrossRef](#)]
16. Agrebi, Y.; Koubaa, Y.; Boussak, M. Rotor Resistance Estimation for Indirect Stator Oriented Induction Motor Drive Based on MRAS Scheme. In Proceedings of the 10th International Conference on Sciences and Techniques of Automatic Control & Computer Engineering, Hammamet, Tunisia, 20–22 December 2009; Academic Publication Center of Tunis: Hammamet, Tunisia, 2009.
17. Parasiliti, F.; Petrella, R.; Tursini, M. Adaptive Sliding Mode Observer for Speed Sensorless Control of Induction Motors. In Proceedings of the Conference Record of the 1999 IEEE Industry Applications Conference. Thirty-Forth IAS Annual Meeting (Cat. No.99CH36370), Phoenix, AZ, USA, 3–7 October 1999; IEEE: Piscataway, NJ, USA, 1999; Volume 4, pp. 2277–2283.
18. Sahraoui, K.; Kouzi, K.; Ameer, A. Neural Networks Trained with Sliding Mode Control for DSIM Supplied by Two Voltage Inverters on Three Levels. In Proceedings of the 2018 International Conference on Electrical Sciences and Technologies in Maghreb (CISTEM), Algiers, Algeria, 28–31 October 2018; IEEE: Piscataway, NJ, USA, 2018; pp. 1–6.
19. Yang, S.; Sun, R.; Cao, P.; Xie, Z.; Zhang, X. Sliding-Mode Observer Based Rotor Resistance Updating Method for Indirect Vector Controlled Induction Motor. In Proceedings of the 2017 IEEE Transportation Electrification Conference and Expo, Asia-Pacific (TEC Asia-Pacific), Harbin, China, 7–10 August 2017; IEEE: Piscataway, NJ, USA, 2017; pp. 1–5.
20. Kubota, H.; Matsuse, K.; Nakano, T. DSP-Based Speed Adaptive Flux Observer of Induction Motor. *IEEE Trans. Ind. Appl.* **1993**, *29*, 344–348. [[CrossRef](#)]
21. Jouili, M.; Agrebi, Y.; Koubaa, Y.; Boussak, M. A Luenberger State Observer for Simultaneous Estimation of Speed and Stator Resistance in Sensorless IRFOC Induction Motor Drives. In Proceedings of the 2015 16th International Conference on Sciences and Techniques of Automatic Control and Computer Engineering (STA), Monastir, Tunisia, 21–23 December 2015; IEEE: Piscataway, NJ, USA, 2015; pp. 898–904.
22. Azzoug, Y.; Menacer, A.; Ameid, T.; Ammar, A. Performance Improvement of Sensorless Vector Control for Induction Motor Drives Using Fuzzy-Logic Luenberger Observer: Experimental Investigation. In Proceedings of the 2019 International Conference on Applied Automation and Industrial Diagnostics (ICAAID), Elazig, Turkey, 25–27 September 2019; IEEE: Piscataway, NJ, USA, 2019; pp. 1–6.
23. Wlas, M.; Krzeminski, Z.; Toliyat, H.A. Neural-Network-Based Parameter Estimations of Induction Motors. *IEEE Trans. Ind. Electron.* **2008**, *55*, 1783–1794. [[CrossRef](#)]
24. Cirrincione, M.; Pucci, M.; Cirrincione, G.; Capolino, G.A. A New Experimental Application of Least-Squares Techniques for the Estimation of the Induction Motor Parameters. *IEEE Trans. Ind. Appl.* **2003**, *39*, 1247–1256. [[CrossRef](#)]
25. Karanayil, B.; Rahman, M.F.; Grantham, C. Stator and Rotor Resistance Observers for Induction Motor Drive Using Fuzzy Logic and Artificial Neural Networks. In Proceedings of the 38th IAS Annual Meeting on Conference Record of the Industry Applications Conference, 2003, Salt Lake City, UT, USA, 12–16 October 2003; IEEE: Piscataway, NJ, USA, 2003; Volume 1, pp. 124–131.
26. Gadoue, S.M.; Giaouris, D.; Finch, J.W. Sensorless Control of Induction Motor Drives at Very Low and Zero Speeds Using Neural Network Flux Observers. *IEEE Trans. Ind. Electron.* **2009**, *56*, 3029–3039. [[CrossRef](#)]

27. Haddoun, A.; Benbouzid, M.E.H.; Diallo, D.; Abdessemed, R.; Ghouili, J.; Srairi, K. Comparative Analysis of Estimation Techniques of SFOC Induction Motor for Electric Vehicles. In Proceedings of the 2008 18th International Conference on Electrical Machines, Vilamoura, Portugal, 6–9 September 2008; IEEE: Piscataway, NJ, USA, 2008; pp. 1–6.
28. Gadoue, S.M.; Giaouris, D.; Finch, J.W. Performance Evaluation of a Sensorless Induction Motor Drive at Very Low and Zero Speed Using a MRAS Speed Observer. In Proceedings of the 2008 IEEE Region 10 and the Third international Conference on Industrial and Information Systems, Kharagpur, India, 8–10 December 2008; IEEE: Piscataway, NJ, USA, 2008; pp. 1–6.
29. Peng, F.Z.; Fukao, T. Robust Speed Identification for Speed-Sensorless Vector Control of Induction Motors. *IEEE Trans. Ind. Appl.* **1994**, *30*, 1234–1240. [[CrossRef](#)]
30. Nitayotan, C.; Sangwongwanich, S. A Filtered Back EMF Based Speed-Sensorless Induction Motor Drive. In Proceedings of the Conference Record of the 2001 IEEE Industry Applications Conference. 36th IAS Annual Meeting (Cat. No.01CH37248), Chicago, IL, USA, 30 September–4 October 2001; IEEE: Piscataway, NJ, USA, 2001; Volume 2, pp. 1224–1231.
31. Maiti, S.; Chakraborty, C. A New Instantaneous Reactive Power Based MRAS for Sensorless Induction Motor Drive. *Simul. Model. Pract. Theory* **2010**, *18*, 1314–1326. [[CrossRef](#)]
32. Manohar, M.; Das, S. Combined Speed and Rotor Resistance Estimation for Speed Sensorless Induction Motor Drive Using Reactive Power Based MRAS. In Proceedings of the Michael Faraday IET International Summit 2015, Kolkata, India, 12–13 September 2015; Institution of Engineering and Technology: Stevenage, UK, 2015; pp. 56–57.
33. Kiran, K.; Das, S. Implementation of Reactive Power-based MRAS for Sensorless Speed Control of Brushless Doubly Fed Reluctance Motor Drive. *IET Power Electron.* **2018**, *11*, 192–201. [[CrossRef](#)]
34. Orłowska-Kowalska, T.; Dybkowski, M. Stator-Current-Based MRAS Estimator for a Wide Range Speed-Sensorless Induction-Motor Drive. *IEEE Trans. Ind. Electron.* **2010**, *57*, 1296–1308. [[CrossRef](#)]
35. Asfu, W.T. Stator Current-Based Model Reference Adaptive Control for Sensorless Speed Control of the Induction Motor. *J. Control Sci. Eng.* **2020**, *2020*, 8954704. [[CrossRef](#)]
36. Ravi Teja, A.V.; Chakraborty, C.; Maiti, S.; Hori, Y. A New Model Reference Adaptive Controller for Four Quadrant Vector Controlled Induction Motor Drives. *IEEE Trans. Ind. Electron.* **2012**, *59*, 3757–3767. [[CrossRef](#)]
37. Das, S.; Kumar, R.; Chattopadhyay, A.K. Comparison of Q- and X-MRAS for Speed Sensor Less Induction Motor Drive On. In Proceedings of the Michael Faraday IET International Summit 2015, Kolkata, India, 12–13 September 2015; Institution of Engineering and Technology: Stevenage, UK, 2015; pp. 319–324.
38. Ide, K.; Ha, J.I.; Sawamura, M.; Iura, H.; Yamamoto, Y. High Frequency Injection Method Improved by Flux Observer for Sensorless Control of an Induction Motor. In Proceedings of the Power Conversion Conference-Osaka 2002 (Cat. No.02TH8579), Osaka, Japan, 2–5 April 2002; IEEE: Piscataway, NJ, USA, 2002; Volume 2, pp. 516–521.
39. Xu, Z.; Shao, C.; Feng, D. An MRAS Method for Sensorless Control of Induction Motor over a Wide Speed Range. *J. Control Theory Appl.* **2011**, *9*, 203–209. [[CrossRef](#)]
40. Xu, L.; Inoa, E.; Liu, Y.; Guan, B. A New High Frequency Injection Method for Sensorless Control of Doubly-Fed Induction Machines. In Proceedings of the 2011 IEEE Energy Conversion Congress and Exposition, Phoenix, AZ, USA, 17–22 September 2011; IEEE: Piscataway, NJ, USA, 2011; pp. 1758–1764.
41. Kojabadi, H.M.; Abarzadeh, M.; Chang, L. A Comparative Study of Various Methods of IM's Rotor Resistance Estimation. In Proceedings of the 2015 IEEE Energy Conversion Congress and Exposition (ECCE), Montreal, QC, Canada, 20–24 September 2015; IEEE: Piscataway, NJ, USA, 2015; pp. 2884–2891.
42. Kumar, R.; Das, S.; Syam, P.; Chattopadhyay, A.K. Review on Model Reference Adaptive System for Sensorless Vector Control of Induction Motor Drives. *IET Electr. Power Appl.* **2015**, *9*, 496–511. [[CrossRef](#)]
43. Tiwari, A.; Kumar, B.; Chauhan, Y.K. ANN Based RF-MRAS Speed Estimation of Induction Motor Drive at Low Speed. In Proceedings of the 2017 International conference of Electronics, Communication and Aerospace Technology (ICECA), Coimbatore, India, 20–22 April 2017; IEEE: Piscataway, NJ, USA, 2017; pp. 176–179.
44. Dehghan-Azad, E.; Gadoue, S.; Atkinson, D.; Slater, H.; Barrass, P.; Blaabjerg, F. Sensorless Control of IM Based on Stator-Voltage MRAS for Limp-Home EV Applications. *IEEE Trans. Power Electron.* **2018**, *33*, 1911–1921. [[CrossRef](#)]
45. Gadoue, S.M.; Giaouris, D.; Finch, J.W. A Neural Network Based Stator Current MRAS Observer for Speed Sensorless Induction Motor Drives. In Proceedings of the 2008 IEEE International Symposium on Industrial Electronics, Cambridge, UK, 30 June–2 July 2008; IEEE: Piscataway, NJ, USA, 2008; pp. 650–655.
46. Venkadesan, A.; Himavathi, S.; Muthuramalingam, A.; Sedhuraman, K. ANN Based Flux Estimator for Rotor Resistance Estimation in Vector Controlled IM Drives. In Proceedings of the 2018 IEEE International Conference on System, Computation, Automation and Networking (ICSCAN), Pondicherry, India, 6–7 July 2018; IEEE: Piscataway, NJ, USA, 2018; pp. 1–5.
47. Krishnan, R. *Electric Motor Drives: Modeling, Analysis and Control*; Pearson Prentice Hall: Hoboken, NJ, USA, 2013.
48. Ajithanjaya Kumar, M.K.; Ballal, R.; Saralaya, S.; Bhat, J.S. Novel Adaptive Learning Rate Back Propagation Neural Network-Based Online Rotor and Stator Resistance Estimator for Sensorless Induction Motor Drives. In *Advances in Communication and Applications*; Shetty, N.R., Prasad, N.H., Nagaraj, H.C., Eds.; Springer Nature Singapore: Singapore, 2024; pp. 557–573.
49. Kumar, A.; Bhat, S.; Ballal, R. Experimental Investigations of Load Characteristics of Induction Motor Drive. *IOP Conf. Ser. Mater. Sci. Eng.* **2021**, *1065*, 012046. [[CrossRef](#)]

50. Sengamalai, U.; Anbazhagan, G.; Thamizh Thentral, T.M.; Vishnuram, P.; Khurshaid, T.; Kamel, S. Three Phase Induction Motor Drive: A Systematic Review on Dynamic Modeling, Parameter Estimation, and Control Schemes. *Energies* **2022**, *15*, 8260. [[CrossRef](#)]
51. Da Silva, L.E.B.; Bose, B.K.; Pinto, J.O.P. Recurrent-Neural-Network-Based Implementation of a Programmable Cascaded Low-Pass Filter Used in Stator Flux Synthesis of Vector-Controlled Induction Motor Drive. *IEEE Trans. Ind. Electron.* **1999**, *46*, 662–665. [[CrossRef](#)]
52. Wang, Z.S.; Ho, S.L. Indirect Rotor Field Orientation Vector Control for Induction Motor Drives in the Absence of Current Sensors. In Proceedings of the 2006 CES/IEEE 5th International Power Electronics and Motion Control Conference, Shanghai, China, 14–16 August 2006; IEEE: Piscataway, NJ, USA, 2006; pp. 1–5.

Disclaimer/Publisher’s Note: The statements, opinions and data contained in all publications are solely those of the individual author(s) and contributor(s) and not of MDPI and/or the editor(s). MDPI and/or the editor(s) disclaim responsibility for any injury to people or property resulting from any ideas, methods, instructions or products referred to in the content.